

# Master of Science in Aerospace Engineering



**POLITECNICO  
DI TORINO**

## Master Thesis

# Dual technology structural health monitoring: comparison between independent technologies for a stronger result

Supervisors

Prof. Paolo Maggiore  
Prof. Matteo Davide Lorenzo Dalla Vedova  
Corporate tutor: Lorenzo Grossi

Candidate

Rachele Fausti

March 2019



# Sommario

In questo lavoro di tesi vengono depositate le fondamenta per più approfondite sperimentazioni nel contesto dello Structural Health Monitoring (SHM) che ha la finalità di migliorare e semplificare il monitoraggio delle strutture, non solo in campo aerospaziale. SHM è un nuovo metodo per effettuare prove non distruttive che vuole dare un giudizio sullo stato dei componenti durante il ciclo di vita operativo. Lo stato di un componente deve rimanere in un dominio specificato in fase di progettazione, sebbene possa essere alterato dall'ambiente circostante, dal normale invecchiamento dei materiali o da eventi accidentali. Dotare i componenti di elementi sensoristici accurati costituisce uno step obbligato per favorire la creazione di materiali e strutture di una complessità sempre maggiore e renderli adattabili ad ogni situazione. Il lavoro di tesi è stato elaborato in sinergia tra Politecnico di Torino e l'azienda Progem. In particolare, Progem si occupa di industrializzazione, produzione e controllo di parti meccaniche di precisione per l'industria aerospaziale, spaziale e della difesa sia per scopi civili che militari, oltre ad essere un fornitore Tier1 che progetta, produce, assembla e collauda strutture e componenti sia per l'industria aerospaziale che della difesa. L'azienda è impegnata in diversi progetti di ricerca e sviluppo nel settore aerospaziale, con il supporto del Politecnico di Torino e di alcune grandi aziende piemontesi; ciò ha reso possibile lo sviluppo della ricerca di cui si andrà a parlare nel corso dell'elaborato. Lo scopo di tale studio è quello di porre in relazione i risultati provenienti dal sensore in fibra di carbonio In-C, sviluppato dall'azienda Progem, con i dati provenienti dal sensore in fibra ottica con reticoli di Bragg già validato grazie ad una precedente ricerca. Per soddisfare l'obiettivo prefissato sono stati condotti dei test di pura flessione su un provino in acciaio armonico con la finalità di misurarne la deformazione. Per dare completezza ai risultati ottenuti sono state ricavate le deformazioni tramite la teoria della trave di Eulero-Bernoulli e tramite simulazioni con il software Patran.

# Summary

In this thesis work, the foundations are laid for more in-depth experiments in the context of Structural Health Monitoring (SHM), which aims to improve and simplify the monitoring of structures, not only in the aerospace field. SHM is a new method to carry out non-destructive evaluations in order to estimate the state of the components during the operating life cycle. The state of a component must remain within a domain specified at the design stage, although it may be altered by the surrounding environment, normal aging of materials or accidental events. Providing the components with accurate sensor elements is an essential step to allow the development of materials and structures of increasing complexity and make them adaptable to any situation. The thesis work was developed in cooperation between the Polytechnic of Turin and the company Progem. In particular, Progem deals with the industrialization, production and control of precision mechanical parts for the aerospace, space and defence industries for both civil and military purposes, as well as being a Tier1 supplier that designs, produces, assembles and tests structures and components for both the aerospace and defence industries. The company is engaged in various research and development projects in the aerospace sector, with the support of the Polytechnic of Turin and some large Piedmontese companies; this has made possible the further development of the study that will be discussed during the course of the paper. The purpose of this study is to establish a relationship between the results from the In-C carbon fiber sensor, developed by Progem, and the data from the fiber optic sensor with Bragg gratings, already validated through previous research. In order to satisfy the target set, pure bending tests were carried out on a sample in harmonic steel with the aim of measuring the deformation. To give a complete picture of the results obtained, the deformations were determined using Eulero-Bernoulli's beam theory and simulations with the Patran software.



# Contents

<b>List of Figures</b>	4
<b>List of Tables</b>	6
<b>1 Introduction to structural health monitoring</b>	7
1.1 Fiber Optic Sensor System for SHM . . . . .	9
1.1.1 Materials and Geometry of Optical Fibers . . . . .	10
1.1.2 Fiber Bragg gratings sensors . . . . .	13
1.1.3 Production technology of the FBGS . . . . .	16
1.2 Prior Art . . . . .	18
1.2.1 In-C Sensor . . . . .	19
1.2.2 Method for manufacturing the In-C sensors . . . . .	20
1.2.3 Physical principles behind In-C sensors . . . . .	21
1.3 Objectives . . . . .	22
<b>2 Design of the test bench</b>	23
2.1 Vibration isolation system . . . . .	23
2.2 Fiber Bragg's gratings Interrogator . . . . .	24
2.3 Optical fibers . . . . .	24
2.4 Supports for both the handler and sensors . . . . .	26
<b>3 Bonding Tests</b>	30
3.1 New bonding method . . . . .	32
3.1.1 Bonding verification . . . . .	34
3.1.2 Limitations and improvements . . . . .	35
<b>4 Tests and Results</b>	37
4.1 Required software . . . . .	38
4.2 Patran model . . . . .	40
4.3 Fiber Bragg grating sensors results . . . . .	41
4.3.1 Eulero-Bernoulli . . . . .	43
4.3.2 Optical lever . . . . .	44
4.4 In-C sensor results . . . . .	45
4.5 Conclusions and future developments . . . . .	46
<b>Bibliography</b>	49
<b>A Drawings</b>	50
<b>B Strain2</b>	70

# List of Figures

1.1	Principle and organization of SHM system [3]	8
1.2	Example of optical fiber structure	10
1.3	Different types of fibers	12
1.4	Main angle of a fiber optic	13
1.5	Reflection grid	14
1.6	Main characteristics of the fiber Bragg grating sensor	16
1.7	Wavelength displacement due to the application of a load	16
1.8	Draw Tower Gratings	17
2.1	Breadboard used for assembly the test bench	24
2.2	SmartScan	24
2.3	Manual cleaver	25
2.4	Automatic cleaver	25
2.5	Fiber optic position inside the splicer	26
2.6	Splicing process and losses visualization	26
2.7	PRG.PLT.002P: visualization of the plate with the In-C sensors which must be subjected to bending	27
2.8	This image shows the T-support that binds the rod to the breadboard (on the left) and the stopper used to staple the rod to the T-support (on the right)	27
2.9	The first block (front view on the left and rear view on the right) will be used to lock the handler and keep it at a certain height. The second support (front view on the left and rear view on the right) is required to attach the handler to the workbench.	28
2.10	L-shaped support (on the left) and spherical head pusher (on the right)	28
2.11	On the left: assembly of the system that includes the handler. On the right: assembly of the supports necessary to keep the plate in position, which is subject to bending.	29
2.12	Assembly of all elements that made the test bench	29
3.1	Gluing test verification: in the figure on the left is shown the plate with the In-C sensors (sensor on the right) and two optical fibers (sensor on the left), in the figure on the right is shown a phase of the bonding test	31
3.2	Bonding test results	32
3.3	Gluing detail: as evidenced in correspondence of the red mark the glue is not in enough quantity to keep the sensor still	32
3.4	Bonding removal	33
3.5	Representation of the gluing method	33
3.6	Materials testing	34
3.7	result with the new bonding method	34

3.8	Phases of the gluing the new fibers . . . . .	35
3.9	Bonding test results . . . . .	35
4.1	<i>SmartSoftSSI</i> software screen: main window . . . . .	38
4.2	Screen of the <i>Basic Acquisition</i> window of the <i>SmartScanSSI</i> software . . . . .	39
4.3	Main screen of the <i>RF-Monitor</i> software. . . . .	39
4.4	Detail of the window showing the measurements (top), zoom of the graph representing the raw data measured by the sensor (bottom) . . . . .	40
4.5	Patran model of the rod with the application of constraint (blue arrows) and load (yellow arrows) . . . . .	41
4.6	Model of the deformed rod: the positions of the sensors are shown in white . . . . .	41
4.7	Graphic result obtained through the code Post.processing.3.0 that represents the course of the strain during the test . . . . .	42
4.8	In blue are represented the strain values coming from the simulation with Patran, in pink the results coming from the optical fiber . . . . .	42
4.9	Optical lever test scheme, the laser is indicated in red . . . . .	44
4.10	Graphic representation of the data measured by the In-C sensor during the tests . . . . .	45
4.11	Comparison of the trend of the deformations transformed by coefficient (in purple) and by the calibration curve (in blue and in purple) that binds LSB and microstrain . . . . .	46
4.12	Graphic representation of the data collected by the In-C sensor . . . . .	47
4.13	Comparison of the deformations measured by the optical fiber at a distance of 1 day . . . . .	48

# List of Tables

4.1	Summary of results between Patran model and fiber optics with Bragg gratings . . . . .	42
4.2	Summary of results between Patran model and fiber optics with Bragg gratings and the theory of the elastic line . . . . .	44

# Chapter 1

## Introduction to structural health monitoring

Since the end of the 1980s, the concept of smart or intelligent materials and structures has become more and more present in the minds of engineers. These new ideas were particularly welcomed in the fields of aerospace and civil engineering. The concept of Smart Materials/Structures can be considered as a step in the general evolution of man-made objects. There is a continuous trend from simple to complex in human production, starting from the use of homogeneous materials, supported by nature and accepted with their natural properties, followed by multi-materials in particular, composite materials, allowing us to create structures with specific properties. In effect, almost all achievements in this field are only intended to make materials and structures controllable, by embedding sensors. In this context it is possible to include Structural Health Monitoring. Structural Health Monitoring (SHM) is an improve and a new way to make a Non Destructive Evaluation (NDE); it aims to give, at every moment during the life of a structure, an evaluation of the state of the materials, of the different parts constituting the structure as a whole. The state of the structures must remain in the domain specified in the design, although this can be altered by the action of the environment, by the normal aging due to usage and by accidental events [3]. A SHM strategy consists of many important components including sensing network, possibly smart materials, data transmission, data processing and analysis, damage assessment and decision making [3]. SHM has the great potential to offer significant economic and life-safe benefits and this technology is deal with monitoring the structural health of aircraft, buildings and dams; improving the efficiency of turbines and industrial equipment, and much more. This is schematically presented in the figure below, where the organization of a typical SHM system is given in detail.

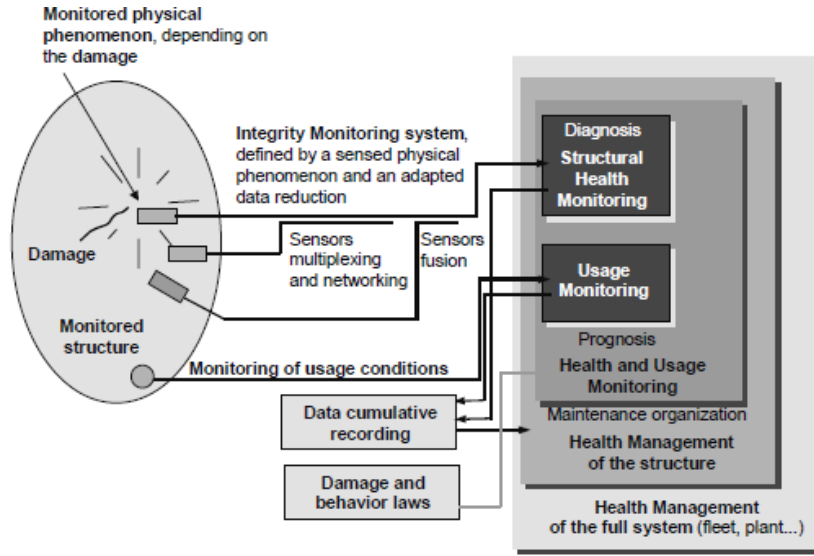


Figure 1.1. Principle and organization of SHM system [3]

The first part of the system, which corresponds to the structural integrity monitoring function, can be defined by: the type of physical phenomenon which is monitored by the sensor and the type of physical phenomenon that is used by the sensor to produce an electric signal sent to the acquisition sub-system [3]. Several sensors of the same type, constituting a network, can be multiplexed and their data merged with those from other types of sensors. Possibly, other sensors, monitoring the environmental conditions, make it possible to perform the usage monitoring functions [3]. The signal derived by the integrity monitoring sub-system, in parallel with the previously registered data, is used by the controller to create diagnostic. Mixing the information of the integrity monitoring sub-system with that of the usage monitoring sub-system and with the knowledge based on damage mechanics and behaviour laws makes it possible to determine the health management of the structure: organization of maintenance, repair operations, etc. Knowing the integrity of in-service structures is a very important objective for manufacturers, end-users and maintenance teams. In effect, SHM:

- allows an optimal use of the structure and the avoidance of catastrophic failure;
- gives the constructor an improvement in his product;
- drastically changes the work organization of maintenance services.

The economic motivation is stronger, especially for end-users. In effect, for structures with SHM systems, the envisaged benefits are constant maintenance costs and reliability, instead of increasing maintenance costs and decreasing reliability for classical structure without SHM [3].

## 1.1 Fiber Optic Sensor System for SHM

In recent years, Fiber Optic Sensors (FOS) have proved to be a potentially excellent technique for real-time *in-situ* monitoring of structures due to their numerous advantages [4]. FOS technology can be used to observe in real time a variety of critical parameters: strain, shape deformation, temperature and strength. This is deal for many utilizations in different discipline.

### **Aerospace**

- Real time structural monitoring for complex bending modes of in-flight aircraft;
- monitoring temperature, strain, load and cryogenic liquid levels in aerospace launch vehicles;
- monitoring thermal/structural health of satellites;
- flight testing;
- aeroelastic feedback control;
- structural configuration;
- embedded fiber design and observing;
- maintenance scheduling;
- end of life cycle decision.

### **Energy**

- Strain, shape and temperature monitoring of next generation seismic processing instruments used for exploration of future drill sites;
- temperature and liquid level monitoring of fluid storage tanks;
- nuclear power plant vibration and temperature monitoring.

### **Transportation and Infrastructure**

- Structural health monitoring of buildings, bridges, dams;
- monitoring the structural health of moving vehicles;
- studying truck and automobile frames.

### **Medical and surgical manoeuvre**

- Robotic surgery;
- biosensing;
- precision biopsy;
- placement and monitoring movements of tiny catheters [4] .

The strong points of fiber optic sensors are easily proven; they are lighter, smaller and can furnish huge numbers of measurements at a fraction of total sensor weight [4]. To achieve these capabilities, the fiber optic sensor system employs Fiber Bragg Grating (FBG) sensors; the real strength of lightweight FBGs resides in its capability to be multiplexed serially [4]. This means that a single optical fiber can contain thousands of Bragg's grating sensors along its length. A narrowband wavelength interrogates the FBG sensors as they respond to deformation resulting from stress or pressure on the structure [4]. Moreover, to accomplish the same number of sensing parts as fiber optic, traditional sensing system would comprise the use of copper wire, coating materials, like plastic and metal.

Fiber optic sensors also have safety benefit because they are chemically inert, they are immune to electromagnetic interference and are not sensitive to sparking or joule heating. These sensors can be embedded within composite materials because of their small size and their pliability.

### 1.1.1 Materials and Geometry of Optical Fibers

The most of common fiber optics are made of glass or plastic material. The choice of the material is given by the purpose of the application. Plastic optical fibers (POF) are used for short-distance application and low-bit-rate transmission systems, because their high attenuation [2]. Therefore, plastic optical fibers are cheaper, more flexible than glass fibers and easy to install and connect [2]. Glass fibers, thanks to their low attenuation, are used for long-distance applications and with systems with a high-bit-rate of transmission. Glass (i.e. Silica) can be doped to increase or reduce the refractive index of the core; the cladding is pure silica [2]. Usually to increase the refractive index are used Germanium dioxide ( $GeO_2$ ), Phosphorus pentoxide ( $P_2O_5$ ), Titanium dioxide ( $TiO_2$ ) and Aluminum oxide ( $Al_2O_3$ ). On the other hand, Boron trioxide ( $B_2O_3$ ) and Fluorine ( $F$ ) can be used to reduce the refractive index [5]. In general optical fibers have a cylindrical geometry and they are characterized by a core, a first cladding and an external coating, as you see in the following figure

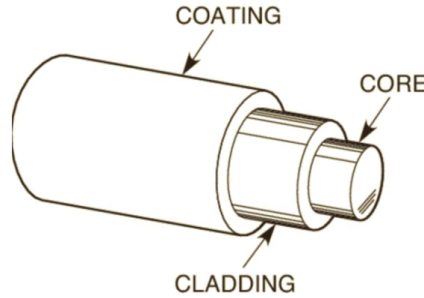


Figure 1.2. Example of optical fiber structure

For example,  $GeO_2$  and  $P_2O_5$  have the peculiarity to increase the refractive index so they are suitable for the fiber core, conversely dopants such as  $F$  and  $B_2O_3$  are suitable for cladding because they reduce the refractive index [1]. If the refractive index of the core is constant, such a fiber is called a step-index fiber. Otherwise the fibers are named graded-index fibers; in this case the refractive index of the cladding is constant and uniform but the refractive index of the core changes gradually, nearly



parabolic, with a maximum value along the axis of fiber until the minimum value along the core-cladding interface.

Consequently, the refractive index of the core is a function of  $r$ , where  $r$  is the radial position. Materials for graded-index fibers, are obtained by adding dopants in a correct concentration [6], and because of this particular variation of refractive index the optical ray does not follow a straight line along the fiber but a curved line. The general function that describes the refractive index variation of graded-index fibers, it is the following relation [6]:

$$n^2(r) = n_1^2[1 - 2(\frac{r}{a})^p \Delta]$$

where  $p$  is called *grade profile parameter* and by varying his value from 1 to  $\infty$  it is possible to obtain different refractive profile, and  $\Delta$  is the *normalize refractive index*. Taking into account the modes of light propagation, optical fibers can be classified in two ways:

- Single-mode fiber optic (SI)
  
- Multi-mode fiber optic (MM)

Single-mode fibers have a small core diameter and only a single pathway or propagation mode for the light; whereas multimode fibers have larger diametric core. In this latter case, the options for the angles at which the light can enter the cable are greater, and so multiple pathways are possible[7]. In fact the SI fiber has a core diameter of 10  $\mu\text{m}$ , instead the MM fiber has a core diameter of about 50  $\mu\text{m}$ . The diameter of the cladding is 125  $\mu\text{m}$  and it is standardised for all types of optical fibers except in some cases.

The multimode is manufactured from plastic whereas the single mode is manufactured from glass [7]; the signals are transmitted in the multimode in a form in which the wave length is varying while in the single mode the wave length remains constant, the diameter of the core varies according to the mode. The refractive index is high in the core while it is smaller in the cladding; this difference causes the refraction of the entering light[7].

Thanks to the large numerical aperture<sup>1</sup> of a multi-mode fiber, more light can be sent inside the fiber by using an inexpensive optical source such a LED [2]. Therefore, this fiber class is easier to splice than single-mode fibers due to its large core. Contrary, multi-mode fiber are not suitable for long haul and applications with a high-bit-rate transmission, because their intermodal dispersion [2]. This phenomenon is a distortion mechanism occurring in multimode fibers and other waveguides, in which the signal is spread in time because the propagation velocity of the optical signal is not the same for all modes. In these case, single-mode fibers are recommended.

---

<sup>1</sup>The *Numerical Aperture* (NA) controls the entering light by measuring the optimum angle of the entering angle of the rays such the total internal refraction could be achieved[7]

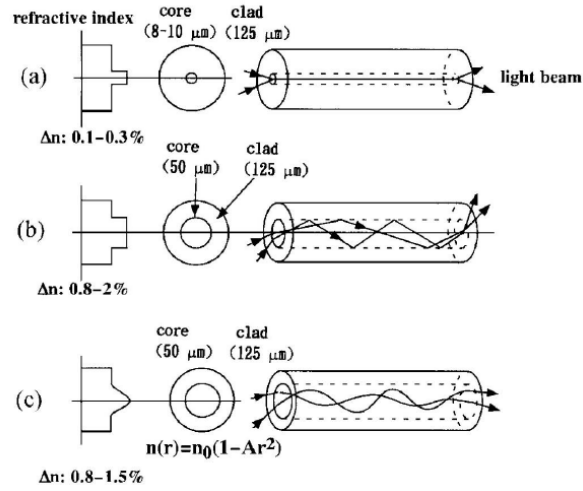


Figure 1.3. (a).Single-mode fiber, (b).MM Step-index fiber, (c).MM Graded-index fiber

The advantages and disadvantages of optical fiber are listed below; for more details refer to the document [10]

#### Strength points

- Thanks to the electrical characteristics of the glass the optical fiber is immune to electromagnetic radiation and lightning strikes;
- unlike metallic materials, glass is chemically stable and has a high melting temperature, so it is resistant to corrosion and high temperatures;
- the optical fiber is smaller and lighter compared to the communication cables, therefore it is easier to install, making the system's sensor component lighter;
- thanks to the signal low attenuation, the fiber optic permits to transmit the signal over long distances;
- the glass that makes up the fiber is easily available;

#### Weak points

- The optical fiber must be installed so that it stands upright or at most with a large radius of curvature, to avoid optical losses;
- fiber construction, use and maintenance costs are high due to expensive interrogation system and instrumentation system for fiber management;
- during the installation phase the fiber is susceptible to mechanical stresses that could damage it, as well as vibration and exposure to humid environments.

### 1.1.2 Fiber Bragg gratings sensors

The propagation of light into the fiber core is based on the Total Internal Reflection (TIR). When the light passes in a region with a refractive index  $n1$  up to one with a lower refractive index  $n2$  it makes a reflection, the angle at which the light enters is specified by the expression (1.1) and, in particular, the light is reflected when  $n1$  is larger than  $n2$  [7]. Refractive index is computed with the following equation:

$$n = \frac{c}{v}$$

- $n$  is the refractive index of the medium taken into consideration;
- $c$  is the speed of light in vacuum;
- $v$  is the speed of light in the considered medium.

The Critical angle is defined by:

$$\sin(\theta_c) = \frac{n1}{n2} \quad (1.1)$$

This angle is obtained from Snell's Law (1.2), when the refractive angle  $\alpha_r$  is  $90^\circ$ .

$$n1 \cdot \sin(\alpha_i) = n2 \cdot \sin(\alpha_r) \quad (1.2)$$

- $n1$  is the refractive index of the first medium;
- $n2$  is the refractive index of the second medium;
- $\alpha_i$  is the incidence angle;
- $\alpha_r$  is the refractive angle.

Beyond this angle, the light is totally reflected. Moreover, the light rays have to pass through the fiber at an angle lower than  $\alpha_{max}$ , so that the light can propagate along the fiber, see fig.(1.4).

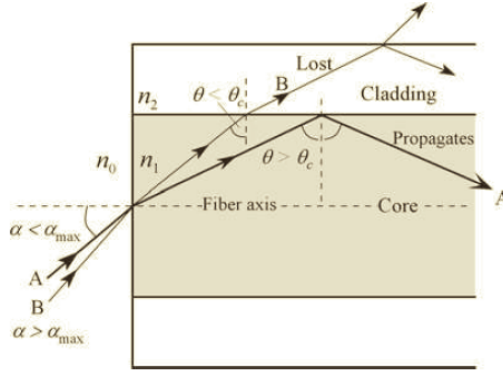


Figure 1.4. Main angle of a fiber optic

The  $\alpha_{max}$  written above is the *maximum acceptance angle*. This angle defines the range in which light can be sent inside the core so TIR can take place, conversely beyond  $\alpha_{max}$ , total reflection does not exist.

In the FBGs, the diffraction grating<sup>2</sup> is achieved by a periodic variation of the fiber core index [9]. The periodic modulation is obtained using a UV light laser, which locally modify the physics property of the material, increasing slightly the refraction index to printing a series of band in the core. This particularly structure is named Fiber Bragg Grating (FBG).

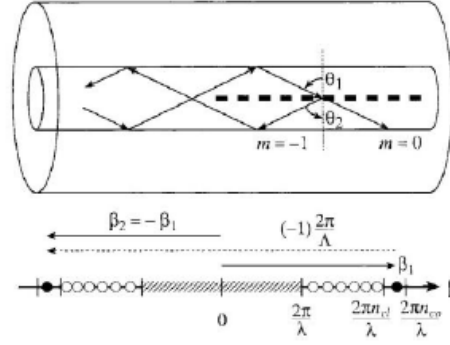


Figure 1.5. Reflection grid

It is possible to determine under what condition is verified a constructive interference for the transmitted and reflected light inside the fiber. In the case of a wave, which propagates itself inside a means with an index of refraction  $n$  not unitary, the equation of maximum constructive interference become:

$$\Lambda n(\sin \theta_2 - \sin \theta_1) = m\lambda \quad (1.3)$$

Where  $\Lambda$  is the grid period. The effective refraction's index for both corners become:

$$n_{eff1} = n \sin \theta_1$$

$$n_{eff2} = n \sin \theta_2$$

And the propagation constant:

$$\beta_1 = n_{eff1} \frac{2\pi}{\lambda}$$

$$\beta_2 = n_{eff2} \frac{2\pi}{\lambda}$$

So the equation become

$$\beta_2 - \beta_1 = m \cdot \frac{2\pi}{\lambda} \quad (1.4)$$

In optical fibers the first order of refraction is the most important, corresponding to  $m = -1$ . Positive values of  $\beta$  correspond to *transmission mode* while the negative one is the *reflection mode*.

<sup>2</sup>*Diffraction gratings*: is an optical component with a periodic structure that splits and diffracts light into several beams travelling in different directions. The emerging coloration is a form of structural coloration. The directions of these beams depend on the spacing of the grating and the wavelength of the light so that the grating acts as the dispersive element[10].

Depending on the direction in which are paired the modes, the gratings can be classified in *Bragg's Grating*, or reflection and transmission grid, also called *Long Period Gratings*.

Limited to the case of reflection grating, the reflection equation can be write:

$$\lambda = \Lambda(n_{eff_1} + n_{eff_2})$$

By demanding the transmission corner is the same of the reflection corner, so  $\theta_1 = -\theta_2$ , we obtained the characteristic relation of a Bragg gratings, giving the wavelength  $\lambda_B$  corresponding the maximum reflected signal:

$$\lambda_B = 2n_{eff}\Lambda \quad (1.5)$$

The dependence of the reflected wavelength to the grating path means that every variation is experienced the path could easily be detected by a wavelength variation. For this reason, the FGB could be used like sensors of deformation and temperature. Furthermore, the linearity of the dependence  $\lambda_B - \Lambda$  is maintained until the sensors breakage and represent a huge advantage in measurement. But a strict translation appears inside the spectre only if we have a uniform variation of the grating path, condition that is verified when the sensor is subjective to a constant stress, mechanical or thermal. If, for example, the sensor is acting on a variable deformation on the grating length, could change also the form of the spectre, making more complex or impossible the identification of the deformation. With a linear deformation, however, the variation of the Bragg's wavelength gives the average deformation on the sensor. The reflected power increases with the sensor's length, from the moment that also increase the number of reflections that the light experienced.

In case of mechanical or thermal tests, a shift of this wavelength occurs. In particular, the equation that considers the contribute of strain and temperature variations is the following equation:

$$\Delta\lambda_B = \lambda_B[(\alpha_f + \zeta_f)\Delta T + (1 - P_e)\epsilon] \quad (1.6)$$

Where

- $\lambda_B$  is the Bragg's wavelength;
- $\epsilon$  is the strain;
- $\Delta T$  is the temperature variation;
- $\zeta_f$  is the thermo-optic coefficient;
- $\alpha_f$  is the thermal expansion coefficient of the fiber optic;
- $P_e$  is the photoelasticity constant.

An illustrative image about the fiber Bragg grating is shown in the figure (1.6).

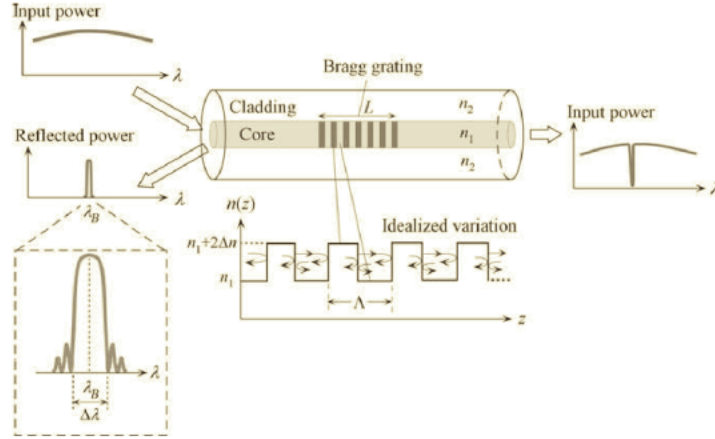


Figure 1.6. Main characteristics of the fiber Bragg grating sensor

By applying a load, because of the variation of the properties of the grating, a wavelength shift occurs, as can be seen in the figure below:

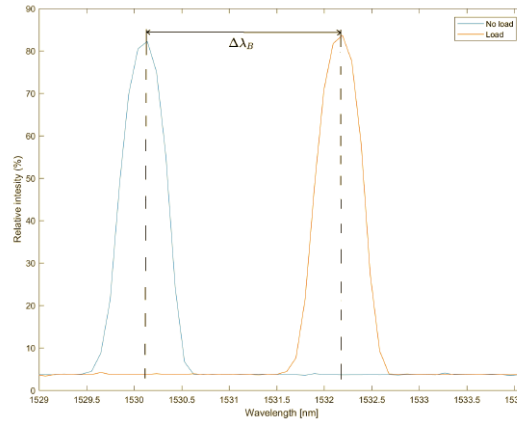


Figure 1.7. Wavelength displacement due to the application of a load

### 1.1.3 Production technology of the FBGS

In a traditionally process of production, the fiber is initially spun and covered with the coating. The coating not permit the transition of the light so the portion destined to the inscription is treated to remove the coating (stripping) and after is exposed to a UV laser that locally modify the refraction index of fiber to inscribes the grating. At the end of the process the part treated is covered with a new coating (recoating). This method, used for the most part of sensors production, weakened the fiber in the point where the coating is removed, reducing the reliability of the sensors. This problem is critical in the production of sensors array because the stripping and recoating area could be more extended, increasing the probability of a create fault. The Draw Tower

Gratings sensors are instead inscribed directly after the process of spinning of the fiber and before deposition of the coating, as illustrated in the figure below.

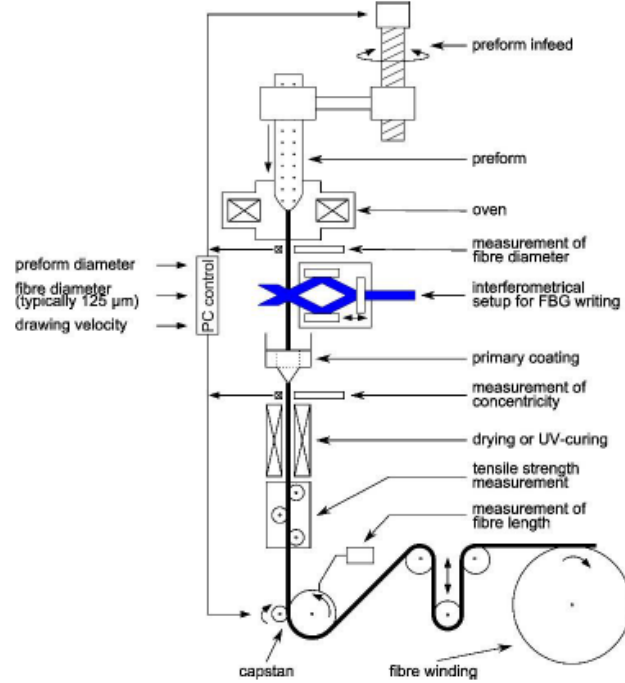


Figure 1.8. Draw Tower Gratings

In this way the mechanical properties of the original fiber are kept.

In the past, the grating produced with this technique presented very low reflectivity, due to the exposure time limit due at high fiber spinning speed. In recent years, thanks to the use of materials with higher photosensitivity and better process control, which allows lower spinning speeds, it became possible to obtain gratings with reflectivity of 30-50%.

This innovative technology presents several advantages compared to a traditional production process:

- High mechanical strength: the coating is placed on the fiber after the grating inscription, so operations of stripping and recoating of traditional processes are unnecessary. In this way the mechanical resistance of the sensor is up to 5 times greater of a traditional sensor.
- Possibility of producing arrays of sensors: this procedure allows to create easily very long arrays without discontinuity between a sensor and the next, and without glue more fibers in sequence (splice less array). The minimum distance between the centers of two gratings, and therefore the spatial resolution of the sensor, is limited to 10 mm due the spinning speed. Varying the length of the individual sensors and their wavelength it is possible to obtain spectra with characteristics different depending on the needs.
- Low cost: being a completely automatic process, the costs of arrays of sensors are relatively small, slightly higher to those of a single sensor obtained with

traditional processes.

## 1.2 Prior Art

The likelihood of identifying and monitoring the strains of a structure is of main importance in a great number of technical fields, among which the building industry, the automotive industry, the nautical sector, the aeronautical sector. As stated by the state of the art, the detection of deformations is accomplished by employing sensors that are either externally applied to the structure to be monitored or placed inside the structure itself [8].

In the first case, the strain gauges are commonly used.; they are glued to the surface of the structure to be monitored. This solution is subject to serious limitation:

- strain gauges made of metal alloy suffer of structural weakness and this characteristic limits their size, thereby limiting the section of surface on which the deformations are detected;
- the detectors are vulnerable to atmospheric agents;
- the bonding of the sensor to the structure is affected by degradation;
- the wire connection between the sensors and the matching reading instruments restricts the number of sensors that can be actually employed[8].

With regard to the sensors to be integrated into the structures, it is preferable to use optical fiber sensors with Bragg gratings. There are other disadvantages to using this solution:

- a special groove must be inserted in the structure to place the fiber cause a discontinuity in the properties of the component;
- optical fiber sensors with Bragg gratings are very expensive;
- The device that allows the optical fiber to operate requires a wire connection that enter the structure and facilitate the ingress of dust;
- the installation of these sensors inside the structure requires a particular attention because they cannot be moved at a later stage and, since they provide a punctual measurement, it is necessary to choose carefully their position[8].

Furthermore, both strain gauges and optical fiber sensors require the use of weighty and high-priced hardware systems[8]. In order to overcome the above restrictions it has been created a new kind of sensors made of composite material, which contain a conductive part which, if deformed, varies its electrical resistance in proportion to the deformation[8].

In addition to the use of composite material, the wire connection with the reading instruments of the sensor has been removed, allowing a wireless transmission[8].

In theory the proposed solution including the use of composite material sensors for detecting strains combined with electronics capable of remotely transmitting the detected data, results in a series of mechanical and electronic problems, that can hardly be solved.



### 1.2.1 In-C Sensor

The main object of this section is to describe a new designed sensor which can overcome the aforesaid drawbacks, by detecting strains and transmitting data, which can be either applied to the surface of the structure to be monitored or inserted inside said structure. More than that, this type of sensor enables a accurate detection of the deformations, not influenced by errors due to disturbances and positioning of the sensor [8].

This device is composed of 3 layers: in the middle layer are present conductive fibers that vary their electrical resistance according to the applied deformation. These fibres, generally carbon, titanium and polyester fibres (with metal deposition, like nickel), are inserted in a matrix of insulating material such as resin and/or glue, such as vinyl ethers, epoxy resin and polyesters. On the other hand, the outer layers are made of insulating composite material: there is the same resin matrix in which insulating fibers such as glass or polyester (without metal deposition) are inserted [8]. For wireless data transmission, an antenna is inserted in the central layer of the sensor: it transfers the data via radio frequency (RFID) to an external data reading instrument. The energy required by the sensor is supplied by the same antenna that transfers the data, always with radio-frequency communications; therefore, an internal power supply system is not necessary. Among the advantages of this technology it is possible to highlight the following:

- The In-C sensor can be produced according to the desired size and geometry, so compared to strain gauges and optical fiber can detect the deformations on a larger portion of the component under test [8];
- this kind of sensor can be applied both inside the structure and on the external surface of the structure[8];
- Due to the fact that the sensor is made of a composite material it can be laminated on the surface or inside the structure and become an integral part of it.[8];
- thanks to the presence of at least one antenna in the middle layer allows wirelessly communications between the sensor and the reciving systems, by using for example radio-frequency communications;
- the excitation energy can be supplied to the strain sensor at the same time as its interrogation; alternatively it is possible to provide the supplying energy to the strain sensor and interrogate it at different times, providing it at the same time with means for accumulating energy (always supplied from the outside in a wireless way) [8]. It will be evident that the operations of detection and transmission of data described above can take place either continuously or in a discrete manner [8];
- a shielding layer, made of ferritic material, protects the radio-frequency communications from disturbances due to eddy currents [8]. Since the radio-frequency communication between the device and the external instrument takes place at short distance, the magnetic component in the radio-frequency emission is of major importance. The presence of conductive materials (carbon, reinforced concrete, metals, and so on) in the structure to which the device is applied near the antenna disturbs or cancels the communication, because of eddy currents generated by the radio-frequency emission in such materials. These eddy currents in turn generate a magnetic field symmetrical and opposite to that of the radio-frequency emission, which is therefore attenuated or canceled [8].

### 1.2.2 Method for manufacturing the In-C sensors

The method for manufacturing this new class of sensors includes at least the steps of:

1. create the first layer of composite material comprising insulating fibres;
2. leave, on the first layer, one strain sensor, an electronic circuit, comprising an electric resistance for detecting changes in the electrical parameters of the strain sensors and one antenna;
3. connecting the strain sensor and the antenna to the electronic circuit;
4. covering with a second outer layer, identical to the first outer layer.

The three layers are catalyzed together under vacuum and controlled temperature and the device is realized as a single piece, which allows to avoid any displacement and slipping of the strain sensor relative to the surrounding outer layers [8].

There are three options to obtain the strain sensor by using a composite material. According to a first option the strain sensor is obtained proceeding through the following steps:

- create a layer of composite material with conductive fibers;
- impregnating this layer with an electrically insulating resin or glue;
- catalyzing;
- cutting the obtained layer in line with the desire pattern.

The strain sensor thus obtained has a larger hysteresis and tends to maintain its shape when not stressed. Moreover, if the layer of impregnated fibers is catalyzed between two 'peel ply' (a fabric that is applied to the pre-impregnated tissue with epoxy resin in order to homogenize the amount of resin on the surface, avoiding the formation of air bubbles) layers, after their removal it has the optimal surface for the following assembling step [8].

According to a second option, said strain sensor is obtained by the steps of:

- create a layer of electrically conductive fibers;
- impregnating said layer with an electrically insulating resin or glue;
- cutting the obtained layer in line with the desired pattern.

In this case, the strain sensor is arranged between the outer layers without being catalyzed (so-called 'fresh') and it is catalyzed only after being assembled to the outer layers [8]. In this way, the risk of displacement or slipping of the thus obtained strain sensor relative to the outer layers during operation is completely eliminated. In this case it is preferable to provide positioning marks in the outer layers for the correct positioning of the strain sensor before catalysis [8].

According to a third option, the strain sensor is obtained by providing a middle layer of composite material consisting of a matrix containing electrically insulating fibers and by making the electrically insulating fibers of the middle layer locally become electrically conductive by deposition of a metal in line with a desired pattern [8].

In particular, the metal, such as nickel, is deposited on both faces of the middle layer so as to achieve the effect of electric conduction, and this middle layer is then placed between the two outer layers [8]. For example, it is possible to manufacture the

middle layer by using polyester fibers and subsequently deposit nickel on both faces corresponding to the desired geometry for the strain sensor [8]. The advantage of this solution mainly consists in the fact that the middle layer is much easier to handle as it is not complex in shape and its positioning with respect to the outer layers can take place with greater ease [8].

### 1.2.3 Physical principles behind In-C sensors

The In-C sensor, as mentioned in the previous section, is composed by a middle layer, in which at least one strain sensor is embedded; due to the applied load, the sensor presents dimensional changes, which are converted into variation of its electrical resistance. Therefore, it is to all intents and purposes a resistive sensor. Resistive strain gauges are based on the physical principle that the elongation of a threadlike conductor is proportional to its internal resistance. For a threaded conductor, the resistance is

$$R = \rho \frac{l}{A} \quad (1.7)$$

Where  $l$  is the length,  $A$  is the section and  $\rho$  is the electrical resistivity of the material. Differentiating and dividing the above equation by  $R$  results in

$$\begin{aligned} \frac{\delta R}{R} &= \frac{1}{R} \left( \frac{\delta R}{\delta \rho} \delta \rho + \frac{\delta R}{\delta l} \delta l + \frac{\delta R}{\delta A} \delta A \right) \\ \frac{\delta R}{R} &= \frac{\delta \rho}{\rho} + \frac{\delta l}{l} - \frac{\delta A}{A} \end{aligned} \quad (1.8)$$

In the equation (1.8) the term  $\delta \rho / \rho$  represents the change in relative resistivity,  $\delta l / l = \epsilon_l$  is the deformation of the conductor in longitudinal direction and  $\delta A / A$  is the relative variation of section of the conductor itself.

In the case of conductors with a circular cross-section of diameter  $D$  or with square section on the side  $l$  you have:

$$\frac{\delta A}{A} = 2 \frac{\delta D}{D} = 2\epsilon_t \quad (1.9)$$

where  $\epsilon_t$  is the deformation of the conductor in the transverse direction. For a conductor stressed along the longitudinal direction by a state of uniaxial tension  $\epsilon_t$  is related to longitudinal deformation  $\epsilon_l$  from the relationship:

$$\epsilon_t = -\nu \epsilon_l \quad (1.10)$$

where  $\nu$  is the Poisson coefficient of the material.

Replacing equation (1.10) in equation (1.9) results in:

$$\frac{\delta A}{A} = 2\epsilon_t = -2\nu \epsilon_l \quad (1.11)$$

Introducing these considerations in equation (1.8) we obtain:

$$\frac{\delta R}{R} = \frac{\delta \rho}{\rho} + (1 + 2\nu) \epsilon_l \quad (1.12)$$

This expression highlights how the variation of relative resistance  $\delta R / R$  is related to the deformation  $\epsilon_l$  and change in relative resistivity  $\delta \rho / \rho$ . This is how you bind

directly the variation of resistance to longitudinal deformation. This is used in strain gages relationship by making the conductor integral to the surface on which the deformation is to be measured.

## 1.3 Objectives

The aim of this work is to test and compare In-C sensors with the FBG sensors. In order to accomplish this objective, the work has been divided in three fundamental steps:

- To design and manufacture the locking systems to lock the fiber optics and the In-C sensor;
- to assembly the test bench;
- to perform measuring campaigns to test both sensors.

## Chapter 2

# Design of the test bench

This chapter describes the design phase of the elements necessary to carry out the tests on the strain sensors and all the instrumentation used for the acquisition and consequent analysis of the results. The design and assembly of the bench are essential to conduct the tests and analyze the data collected from the experiments on FBG and In-C sensors; in this context, one of the main problems concerns external disturbances that can affect the measurement and produce partially or completely incorrect conclusions. The purpose of the test bench is to produce a strain, which must be read by both sensors. It will be noticed a variation of wavelength in the fiber Bragg and a variation of resistance in the sensor In-C; these differences will be transformed into displacements in order to be compared. The main elements to complete the work table are the following:

- Two optical fibers with three Bragg's gratings each;
- one In-C sensor with the corresponding circuit for the data transmission;
- support system for the sensors;
- moving system with attached motor to produce the deformation;
- interrogator to read the tensional state of the FBG;
- two programs to process data from both sensors.

Some of the elements mentioned above will be described in the following pages, not necessarily in order.

### 2.1 Vibration isolation system

In the tests carried out in previous experiments it was seen that sensors, especially fibers, are susceptible to minimal vibration. These vibrations can be caused by a simple movement of air or by vehicles passing on the road alongside the laboratory;

they more or less seriously compromise the accuracy of the results, so it is important to isolate the experiments from this source of disturbance.

For these reasons, the system for carrying out the tests is properly fixed to the breadboard that has damping properties, see figure (2.1).



Figure 2.1. Breadboard used for assembly the test bench

## 2.2 Fiber Bragg's gratings Interrogator

The tensional state of the fibers is displayed by means of an interrogator called *SmartScan*; in practice, a laser signal is sent inside the fibre and the return signal is analysed in terms of wavelength. The data obtained regarding the reflected wavelength can be displayed on the screen or can be saved in a *.log* file and processed using a Matlab program. This interrogator has four input channels for different optical fibers with 16 possible fiber Bragg's gratings each. The fibers used must have a Bragg wavelength from 1528 nm to 1568 nm.



Figure 2.2. SmartScan

## 2.3 Optical fibers

In order to perform the tests it was decided to use two optical fibers with 3 Bragg gratings each.

The fibers are delivered with a Bragg grating each one, the first fundamental step

is to cut the fibres appropriately and, at a later date, to connect the 3 gratings to a single fibre. Second fundamental step is to join the connector to the fiber to be inserted in the interrogator.

At first it is necessary to remove the fiber coating: in our case, the external coating of the fiber optic, where there is the connector, has been removed mechanically by using a stripper, instead the coating of the fiber optics, where there is the Bragg grating, has been removed by using a heat source and chemistry agent such isoprophyl alcohol, because the coating is made of polyimide.

Once external coating is removed, it is necessary to clean the ends of each fiber and cut off the end with a manual (figure 2.3) or automatic cleaver (figure 2.3). The cleaving process is critical because the ends of each fiber needs to be more perpendicular as possible to the longitudinal fiber axis to avoid optical losses.



Figure 2.3. Manual cleaver



Figure 2.4. Automatic cleaver

Accomplished the cleaning and cutting, a heat shrinkable tube have to be inserted

in one of two fibers. Then, the two fiber optics have to be located inside the splicer correctly in proximity to the electrodes, as shown in the figure below.

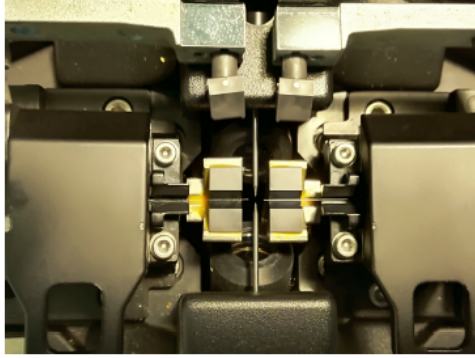


Figure 2.5. Fiber optic position inside the splicer

During the splicing process it can be seen the status of the fiber and the entire process on the monitor. If the cut has been made correctly, the phase of stitching the fibers begins. At the end, an estimate of the losses that could occur after splicing the fibers is displayed on the monitor.

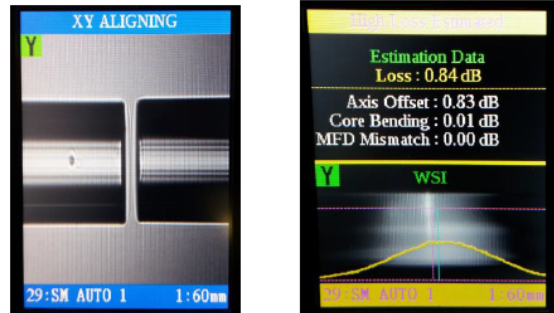


Figure 2.6. Splicing process and losses visualization

## 2.4 Supports for both the handler and sensors

In order to carry out the tests, 7 elements have been designed and modeled using the Catia software, which will form the supports for the sensors and for the handler; appendix A shows the table settings of all components. These include:

- a plate on which the sensors have been glued, which will be subjected to bending by means of a handler. The material chosen for this component is *C72* steel; this is because each harmonic steel component can be deformed up to the elastic limit of the material, without permanent deformation to then return to its initial state.



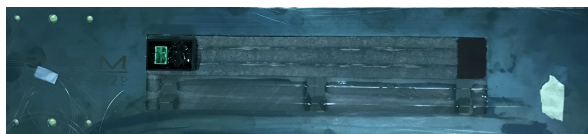


Figure 2.7. PRG.PLT.002P: visualization of the plate with the In-C sensors which must be subjected to bending

- A support and a fastener to bind one end of the plate. In particular, the plate is clamped between the T-shaped support and the stopper by means of 2 screws and a pin so that the constraint is as rigid as possible. The T-bracket is then fixed to the breadboard with 4 more screws.

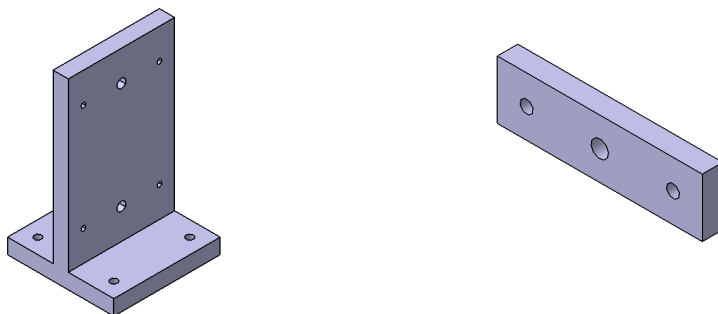
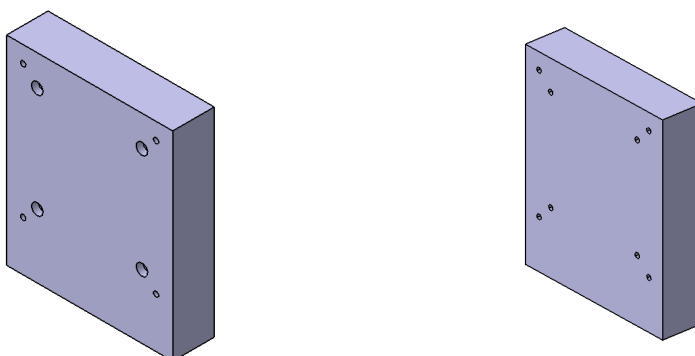


Figure 2.8. This image shows the T-support that binds the rod to the breadboard (on the left) and the stopper used to staple the rod to the T-support (on the right)

- A pair of blocks suitably drilled to support the handler and at the same time secure it to the work bench:



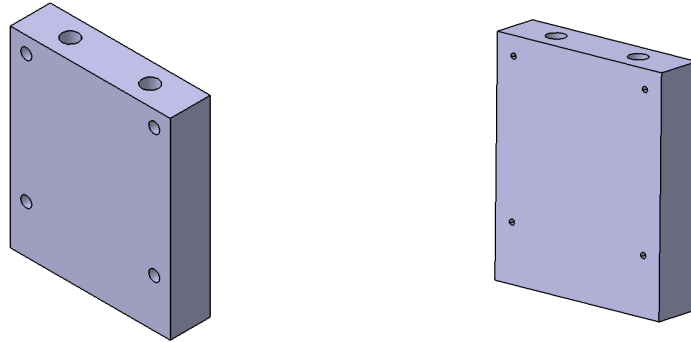


Figure 2.9. The first block (front view on the left and rear view on the right) will be used to lock the handler and keep it at a certain height. The second support (front view on the left and rear view on the right) is required to attach the handler to the workbench

- An L-shaped support and a specially designed ball head screw form the bridge between the handler and the rod. The spherical head screw is the actual pusher which, by moving the handler, deforms the plate. A spherical pusher has been chosen so that there is a single point of contact between the screw and the plate, so that the plate does not undergo a deformation due to contact with the pusher and the displacement will be uniform.

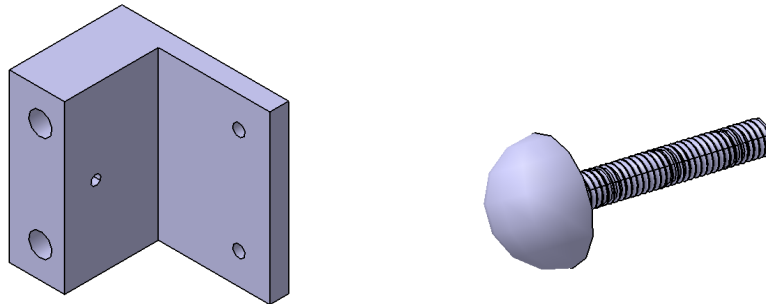


Figure 2.10. L-shaped support (on the left) and spherical head pusher (on the right)

The material used for these supports is aluminum ( $AL6061 - T6$ ) with hard anodic coating ( $MIL - A - 8625f$ ). All components have been designed in such a way as to have a simple geometry to be manufactured in a short time and with minimum costs. In the following images it is possible to visualize the function of the components just described. In particular, in the figure below, on the right, it is possible to identify the support system that has the task of binding the plate as rigidly as possible; in the same figure on the left it is represented the system that has the purpose of supporting the handler (parts in blue and pink) and the pusher composed of the spherical head screw and the L-shaped component (parts in green).



Figure 2.11. On the left: assembly of the system that includes the handler. On the right: assembly of the supports necessary to keep the plate in position, which is subject to bending

The components that hold the handler in place have been designed so that the force applied to bend the plate is applied along the longitudinal axis of the plate itself; so as to have a uniform deformation, avoiding the torsion of the plate.

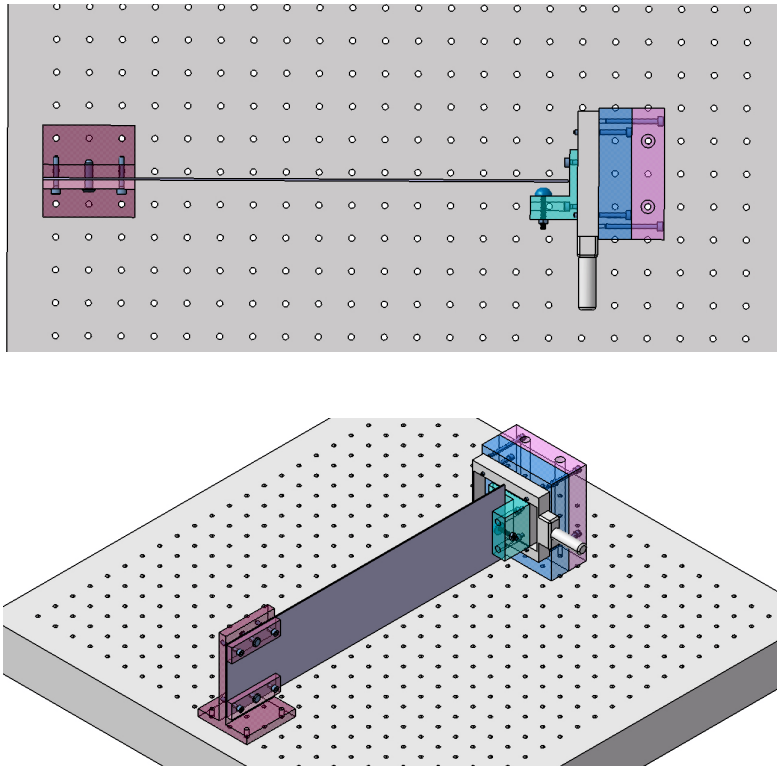


Figure 2.12. Assembly of all elements that made the test bench

## Chapter 3

# Bonding Tests

Before carrying out the tests, it is necessary to verify the tightness of the bonding of the Bragg fibers. The gluing is made by hand following the steps indicated below:

- The component on which the fiber is to be bonded is sanded and then a cloth with alcohol is wiped over the surface to remove any residue and obtain a clean area;
- the fiber is also cleaned with alcohol to eliminate dust;
- a layer of glue, in this case araldite<sup>3</sup>, is spread over the component and then passed with a spatula in order to create a thin layer;
- the fiber is placed on the component and fixed to the sides with a normal adhesive; to obtain a better measure, when the fiber is lowered into the glue, it is pretensioned by hand to make it work only with traction and not in compression. At this stage it is advisable to fix the fibre firmly so that it does not slip during pre-tensioning.

After gluing it is essential to wait at least two days for the glue to dry.

In the figure below on the left you can see the rod with the sensors glued (Figure 3); the free parts (without glue) are the points where the Bragg gratings are placed. It is not strictly necessary to leave the gratings uncovered; in other experiments the fibers have been completely coated and this has not affected the measurements in a compromising way.

With this type of bonding, two types of problems can occur that in one way or another compromise the results.

---

<sup>3</sup> *Araldite* is a two-part epoxy adhesive sets by the interaction of a resin with a hardener. Heat is not necessary although warming will reduce the curing time and improve the strength of the bond. After curing, the joint is claimed to be impervious to boiling water and all common organic solvents. It is available in many different types of packs, the most common containing two different tubes, one each for the resin and the hardener.

1. Firstly, the glue may not be evenly distributed along the entire length of the fiber, so that the sensor may slip inside the glue where it is less thick or in smaller quantities;
2. the second problem is that the layer of glue expands under the fiber. At this point the fiber would no longer be in contact with the component, but is suspended in the layer of glue.

Then, to test the seal of the gluing, the rod was blocked from one end and at the other end a load of 1.28 kg was applied in order to produce a deformation of the component and to tension the sensors, as it can be seen in the figure 3.

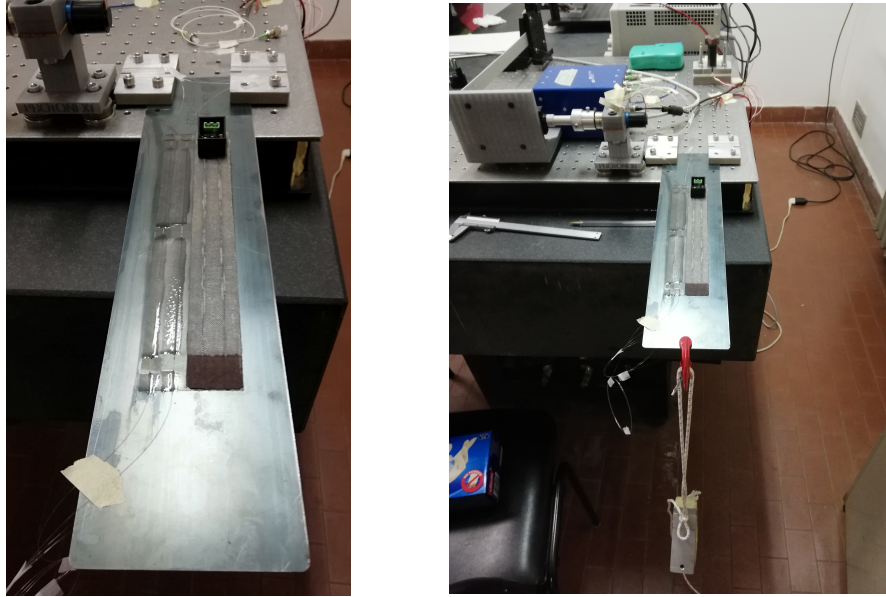


Figure 3.1. Gluing test verification: in the figure on the left is shown the plate with the In-C sensors (sensor on the right) and two optical fibers (sensor on the left), in the figure on the right is shown a phase of the bonding test

In particular, the fibres were connected to the interrogator by means of the appropriate connectors; the rod was kept under tension for about 30 minutes. Through post-processing, the results obtained by printing on the screen the trend of the strain as a function of time can be displayed.

In the graph below it can be seen the trend of the strain of the 3 pairs of Bragg gratings; the grids are numbered starting from those closest to the joint. As represented in the legend of the figure 3.2, *CH* indicates the channel, i.e. the fiber being considered; *GR* indicates the corresponding grating. As already mentioned, there are 3 grids for each fiber; from the graph it is possible to notice that the *GR01* grids of both fibers have an anomalous trend, because being closer to the joint they should measure a higher tension. In addition, during the 30 minutes in which the load is applied, their trend should be more or less constant, without considering disturbances due to vibrations or air displacements. On the contrary, when the load is applied there is a peak, especially with regard to *CH01*, after which the strain drops almost linearly throughout the test time.

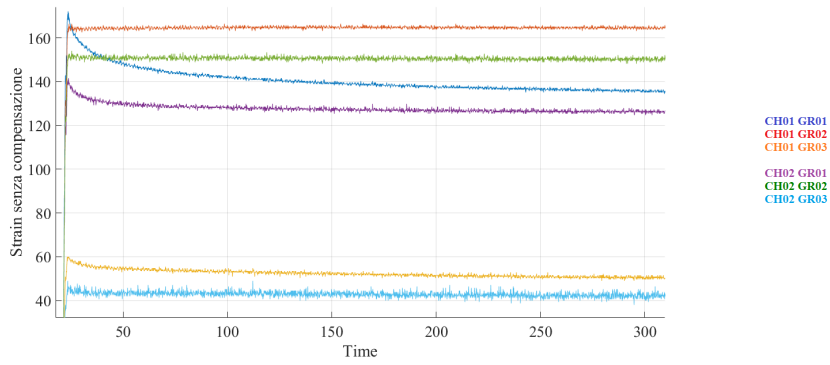


Figure 3.2. Bonding test results

The cause of this behavior is due to the fact that the sensor inside the glue slides and fails to produce a suitable measurement. In fact, as you can see from the picture below, the glue in correspondence of the first Bragg grating is not evenly distributed and the layer is too thin to keep the sensor in position.



Figure 3.3. Gluing detail: as evidenced in correspondence of the red mark the glue is not in enough quantity to keep the sensor still

### 3.1 New bonding method

It was decided to remove the two malfunctioning fibers and replace them with two other fibers consisting of a Bragg grating each, placing the two gratings in different points of the plate. In order to be able to glue the fibers again, it is necessary to remove all the glue using abrasive paper so that no residue remains on the plate.

In figure 3.4 it is possible to see a phase of the gluing removal; part of the glue has been peeled off with a chisel, after which it has been rubbed with abrasive paper to remove any residue.



Figure 3.4. Bonding removal

As the gluing method used was not effective, a new method consisting of the following steps was attempted:

- the surface of the component is sanded and cleaned with alcohol in order to avoid the presence of dust residues;
- a layer of glue is spread with a spatula in the area where the sensor is to be glued;
- the fiber, after having been cleaned with alcohol, is poisoned and stretched on the layer of glue;
- the fibre is compressed with a strip or block of a suitable material that can be easily removed at the end of drying without compromising the bonding.

In fact, by applying a certain continual pressure, it is certain that the fibre sinks completely into the glue and that the layer of glue is sufficiently thin and homogeneous.

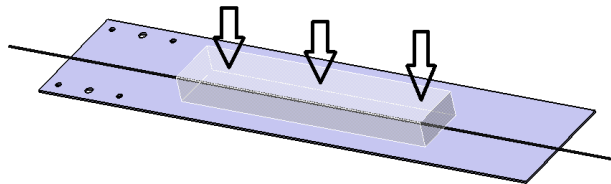


Figure 3.5. Representation of the gluing method

In order to choose the most suitable material, several tests have been carried out

on some plastic materials: PEEK<sup>4</sup>, teflon<sup>5</sup> and POM<sup>6</sup> as in figure 3.1.



Figure 3.6. Materials testing

In particular, a certain amount of glue was poured onto all the pieces and at the end of the drying process, a chisel was used to remove the glue. As you can see, there are no residues of glue left on both teflon and POM, but the force to be impressed with the chisel is too high and, over a larger surface, there is a risk of damaging the entire bonding.

Therefore it was decided to use polyethylene, the classic food grade film, which is placed both under the component to be glued and over the gluing. Lastly, a rather heavy block is placed over the film to ensure sufficient pressure. A test has been carried out to verify the effectiveness of this method; as you can see in the figure, the thickness of the glue is rather homogeneous.



Figure 3.7. result with the new bonding method

### 3.1.1 Bonding verification

The gluing of the new fibres has been carried out as described in the previous paragraph, in figure 3.8 the various phases with the final gluing are shown. After that, the bonding verification test was carried out following the same steps described in paragraph 3.1.

<sup>4</sup>*Poliether ether ketone (PEEK)* is a colourless organic thermoplastic polymer in the polyaryletherketone (PAEK) family, used in engineering applications

<sup>5</sup>*Polytetrafluoroethylene (PTFE)* is a synthetic fluoropolymer of tetrafluoroethylene that has numerous applications. The best known brand name of PTFE-based formulas is Teflon

<sup>6</sup>*Polyoxymethylene (POM)*, also known as acetal, polyacetal, and polyformaldehyde, is an engineering thermoplastic used in precision parts requiring high stiffness, low friction, and excellent dimensional stability



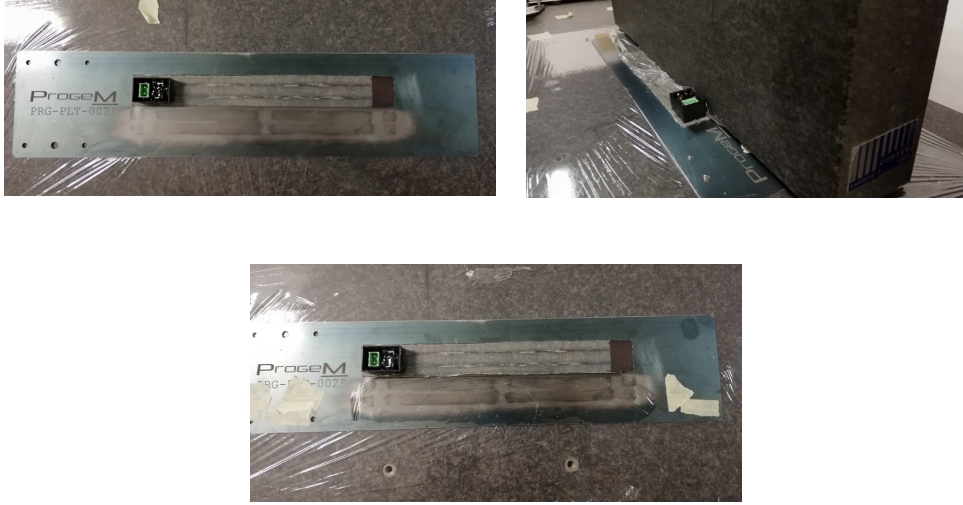


Figure 3.8. Phases of the gluing the new fibers

In this test there are two fibers with a Bragg grating each, positioned in different points of the plate: the grating of channel 1 is positioned towards the joint, while the grating of channel 2 is married to the free end. In addition, the two gratings have been glued in order to have both on the right and on the left of the grating an area large enough to be glued.

The results obtained from the post processing are visible in the graph below: in particular it is noticeable that during the whole time of the measurement the trend of the strain remains constant; this means that the gluing has a firm seal.

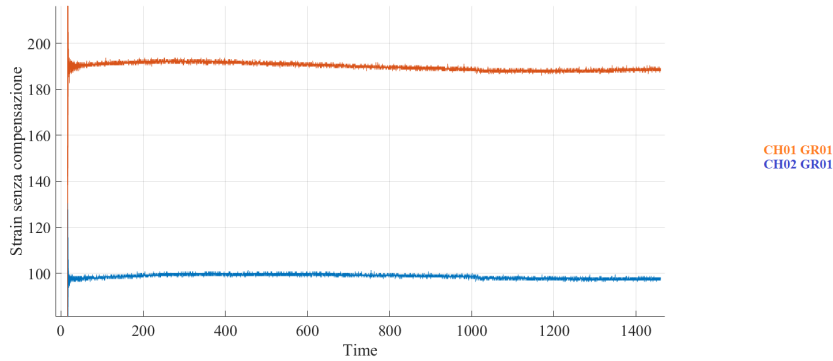


Figure 3.9. Bonding test results

### 3.1.2 Limitations and improvements

This method can be studied and improved from different points of view. First of all, there is no method to define the right amount of glue required for each fiber; the risk would be to have too little glue and compromise the fiber.

Moreover it is necessary to check what weight the block must have to compress the

glue so as not to risk breaking the fiber. In the same way it is probable that the weight of the block when the glue is pressed and expands, causes the fiber to shift. It is important that at the point where the Bragg grating is located the fiber is stretched to ensure the reflection of the signal. For this reason, the block must be positioned vertically on the gluing and the fiber must be well tensioned. In addition, with the gluing method previously used (air drying) the glue is not completely polymerised and to the touch it is rubbery; on the contrary, with this new method the layer of glue is smooth and not gummy.

## Chapter 4

# Tests and Results

The purpose of these tests is to be able to effectively verify that the results of the two sensors: optical fiber with Bragg gratings and In-C, regarding the deformation of the plate, are comparable. The tests were not carried out with the designed supports (see chapter 2) because the manufacturing time did not match the delivery time of the results, so the comparison between the two sensors will be made by binding the plate at one end and applying a load at the free end (see figure 3).

A dozen tests of about 300s each were carried out: the load of 1098g was applied after about 20s from the start of the test. From the moment the load is applied there is a transitional phase due to the oscillations of the weight itself, air movements, etc. After a maximum of 10s the transitory phase is over and there is a more or less linear trend.

In the following paragraphs it will be described the part of the software needed to read the data and measurements. Then the data coming from both sensors will be analyzed; the main problem has been to compare the two types of data because the sensor with Bragg grating provides a measure of the punctual strain, based on where the grating is positioned; it also automatically indicates the strain. On the other hand, the resistive sensor makes readings over the whole length over which it is applied and gives as a result an average of the measurements. Therefore, in order to verify that the two sensors are comparable, a model of the experiment on the *Patran* software has been created and the results obtained with the two sensors will be compared with this model.

## 4.1 Required software

In order to read the data collected by both sensors, it was necessary to use two different software. The *SmartScanSSI* software has been used to measure the Bragg fiber, the main page of which is shown in the following image:

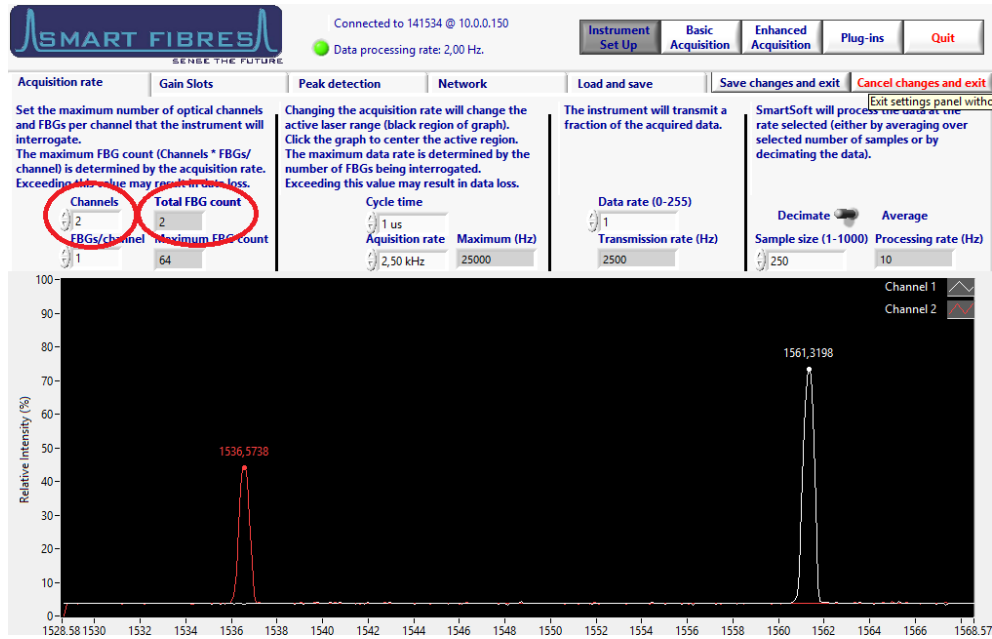
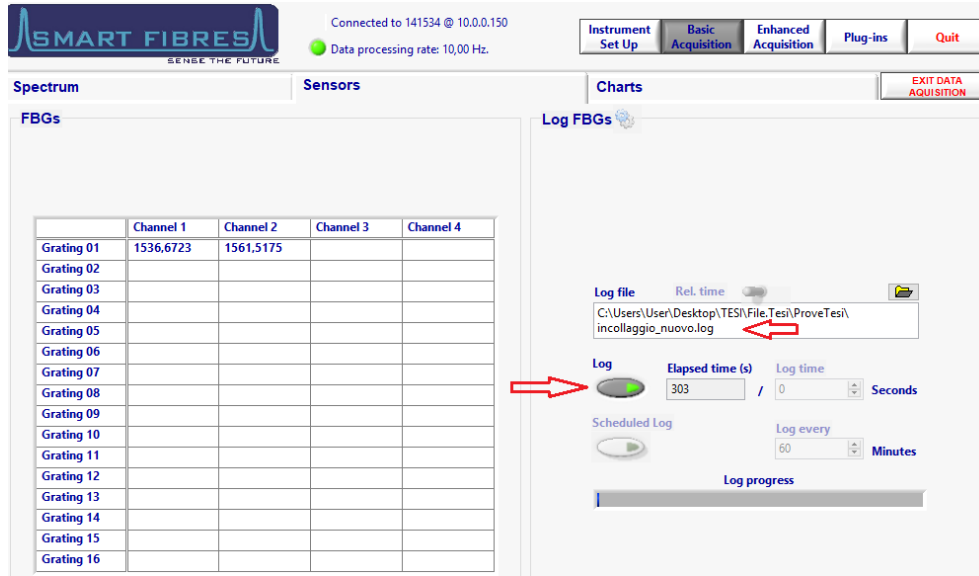


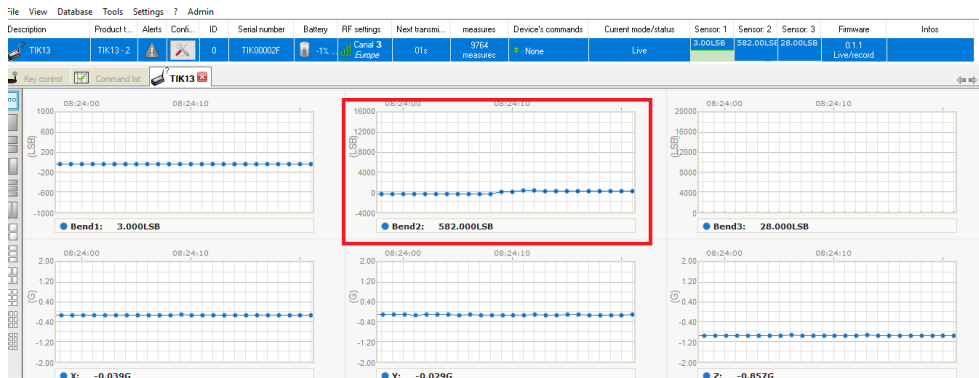
Figure 4.1. *SmartSoftSSI* software screen: main window

It is necessary to insert the number of the considered channels, namely how many fibres you want to connect to the interrogator (it is possible to connect up to a maximum of 4), in our case there are 2 fibers; in the same way, the number of grids present on each fiber must be inserted, therefore from a minimum of 1 to a maximum of 64 (maximum value characteristic of the interrogator being used). After configuring the interrogator, the characteristic wavelengths of each fiber will be printed on the screen, with a distinction between the channels.

In the second screen, called *Basic Acquisition*, it is possible to create a file with *.log* extension in which will be saved all the wavelength values recorded during the tests, this file will be read by the post-processing program in order to produce the trend of the deformation or the wavelength. Pressing the *Log* key it is possible to start the recording of the measurements, checking their timing.

Figure 4.2. Screen of the *Basic Acquisition* window of the *SmartScanSSI* software

To read the data of the In-C sensor, the *RF-monitor* software is used. In figure 4.1 it is possible to display the main window of the program where the name of the sensor (*TIKZ – 13*) and all the transmission characteristics, battery level, quantity of measurements carried out are available. Instead, the diagrams reproduce in real time the raw data read by the sensor as time passes. There are 3 acquisition bands, the one relating to the sensor that will be used is the number 2. Before testing with this software it is necessary to configure the "zero"; after that it is possible to start the data recording. As said, the recorded values are raw data, so in order to obtain the strain we are interested in, it is necessary to carry out a conversion through a curve.

Figure 4.3. Main screen of the *RF-Monitor* software

The results are represented graphically as in the following figure. As already mentioned, they are raw data and each point of the graph represents the average of what the sensor measures on the surface on which it is applied. Similarly, when the data is converted into microstrains, each converted point will represent the average of the deformation on the plate. Once the page where the measurements are printed is open, it is necessary to select the name of the sensor, the transmission band and the acquisition period to be displayed.

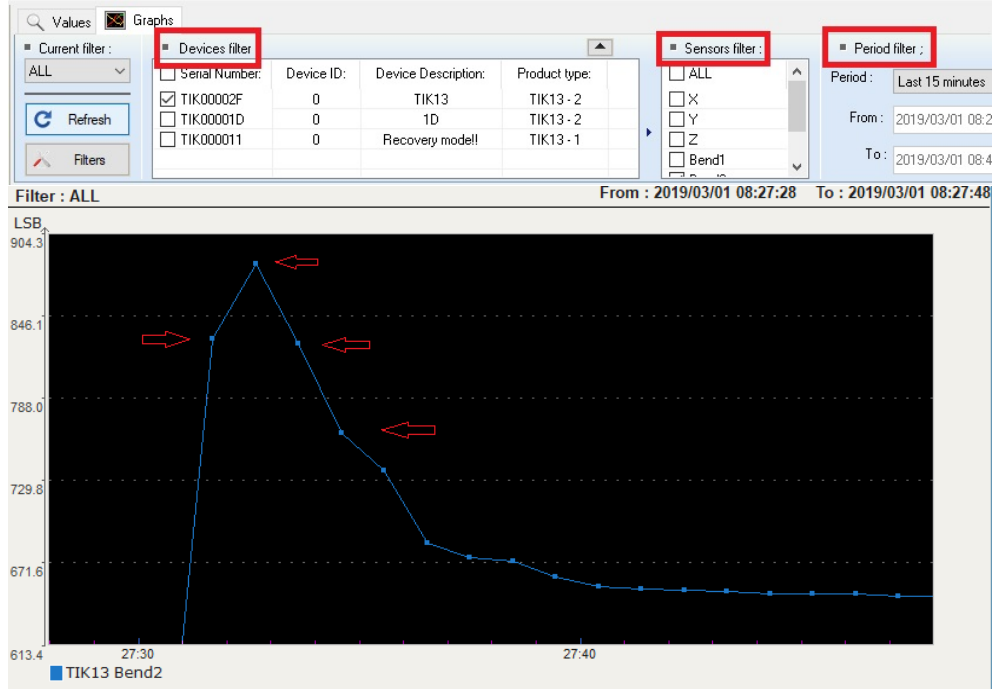


Figure 4.4. Detail of the window showing the measurements (top), zoom of the graph representing the raw data measured by the sensor (bottom)

The collected data can also be saved in excel files.

## 4.2 Patran model

The rod model with Patran software was made to compare the deformation given by the sensors with that of the software because a direct comparison was not possible. The software reported the exact measurements of the rod used, the material used and its characteristics (modulus of elasticity, density), after which a constraint was added (in the image shown with the blue arrows) corresponding to the constraint used in the real experiment. At the free end the load was modeled with the application of a force corresponding to 1098 g (in the image indicated with the yellow arrows): the load is applied by means of a clamp at the centre of the plate at the free end.



Figure 4.5. Patran model of the rod with the application of constraint (blue arrows) and load (yellow arrows)

After the analysis we obtain the model of the rod deformed under the action of the load, as in figure 4.2. In order to be able to compare the data obtained from this analysis with the data coming from the sensors, it was required to indicate on the model the position of both the Bragg gratings and the In-C sensor (indicated in white in the figure); then collect all the strain values corresponding to the elements of the mesh at the position of the sensors.

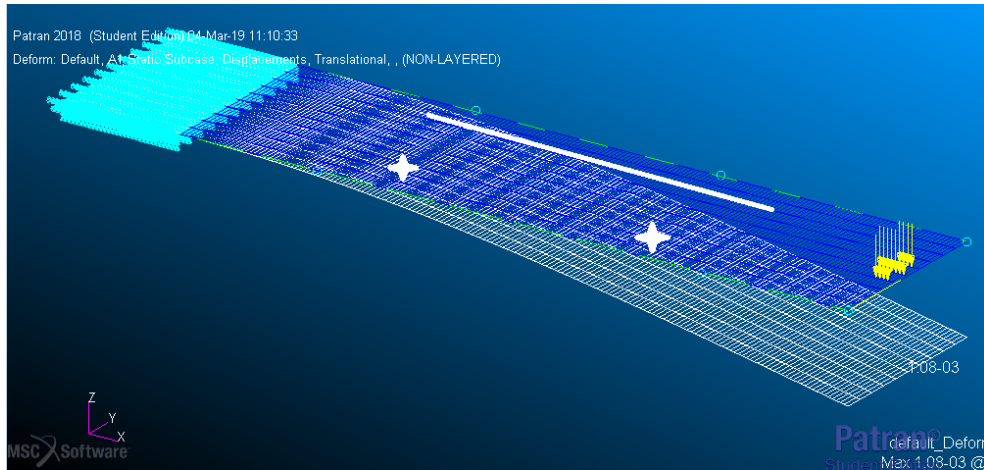


Figure 4.6. Model of the deformed rod: the positions of the sensors are shown in white

### 4.3 Fiber Bragg grating sensors results

The SmartScanSSI software described above creates a *.log* file in which the wavelengths measured during the test are saved; using the Matlab code *Post.Processing.3.0* a graphic result is obtained, showing the strain variation during the test time, figure 4.3. The solution is only graphical so to have the precise value of strain measured, starting from the data saved in the *.log* file, another Matlab code (named *Strain2*, in appendix B) has been written that simply averages the wavelengths measured before and after the application of the load (excluding the transient phase) and then with the formula 1.6 it is possible to obtain the strain.

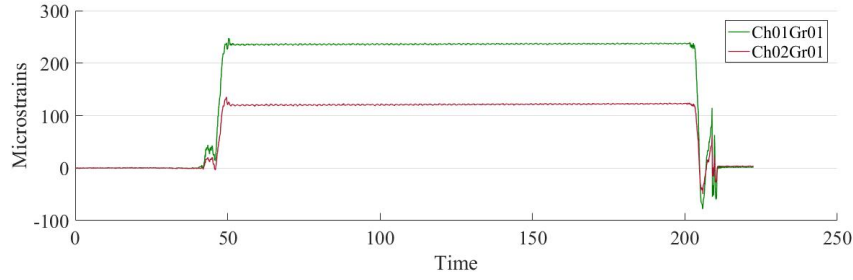


Figure 4.7. Graphic result obtained through the code Post.processing.3.0 that represents the course of the strain during the test

With reference to the previous image we have that the trend of the strain in green corresponds to the Bragg grating positioned near the joint; on the other hand, the trend in burgundy corresponds to the grating near the free end. Using the Strain2 code it was possible to obtain the two strain values, *235microstrains* and *120microstrains* respectively. At this point these strain values were compared with the corresponding results from the Patran model. the results obtained have been plotted in the following diagram; where the strain values resulting from the Patran model are indicated in blue and those measured by the optical fibers are reported in pink.

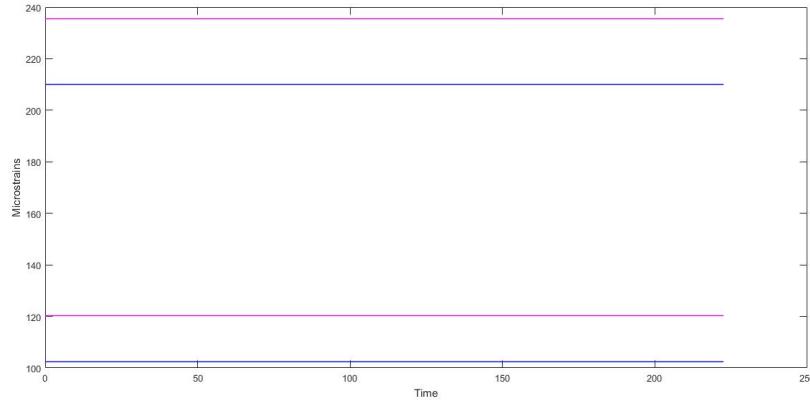


Figure 4.8. In blue are represented the strain values coming from the simulation with Patran, in pink the results coming from the optical fiber

The results are grouped in the following table, the values are measured in microstrains.

Grid position	Patran model $\mu\epsilon$	Optical fiber $\mu\epsilon$
Interlock	210	235
Free end	102	120

Table 4.1. Summary of results between Patran model and fiber optics with Bragg gratings

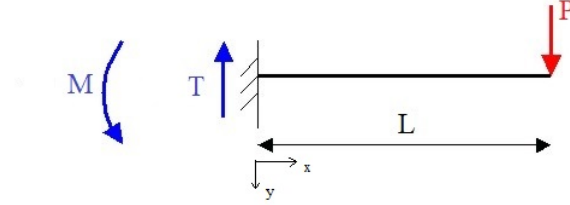


The results can be considered acceptable, considering that in the case of optical fibre the load is not applied instantaneously and is subject to disturbances during the test: air movements, vibrations. The error that occurs is about 10 percent and is due to the fact that the glue continues to polymerize and the fiber tends to rise over the glue itself.

In addition to the Patran test, deflection and deformation were calculated using Eulero-Bernoulli's beam theory and a further an optical lever test was carried out in order to confirm the data from the Patran and fiber optic model; both will be developed in the following sections.

### 4.3.1 Eulero-Bernoulli

In this section are shown the steps to obtain the deflection and deformation through the theory of the elastic line:



$$L = 350 \text{ mm}$$

$$P = 10.77 \text{ N}$$

The bending moment is obtained by using  $M = P \cdot L$ . After that, starting from the connection between moment and curvature, it is possible to calculate the deflection and consequently the strains of the beam.

$$\frac{\delta^2 \nu}{\delta x^2} = -\frac{M(x)}{EI} = \frac{1}{\rho} \quad (4.1)$$

where  $\rho$  is the curvature and  $\nu$  is the deflection;  $E = 206 \text{ kN/mm}^2$  is the elastic module of the material and  $I = 60 \text{ mm}^4$  is the moment of inertia of the beam.

$$\frac{\delta \nu}{\delta x} = -\frac{Mx - \frac{1}{2}Tx^2}{EI} + C_1$$

Where  $T = P$ , the constant  $C_1$  is equal to zero if the boundary condition  $\frac{\delta \nu}{\delta x}$  is introduced at the junction, therefore  $x = 0$ .

$$\frac{\delta \nu}{\delta x} = -\frac{Mx - \frac{1}{2}Tx^2}{EI}$$

Integrating another time results in the displacement:

$$\nu = -\frac{\frac{1}{2}Mx^2 - \frac{1}{6}Tx^3}{EI} + C_2$$

In  $x = 0$  the condition  $\nu = 0$  is set, so  $C_2 = 0$ . To obtain the deflection at the free end it is possible to replace  $x = L$  and  $T = P$  and it is obtained as follows:

$$\nu = -\frac{1}{6} \frac{PL^3}{EI} - \frac{1}{2} \frac{PL^3}{EI} = \frac{1}{3} \frac{PL^3}{EI} = 12.5 \text{ mm} \quad (4.2)$$

The strains are computed as shown below:

$$\epsilon_x(x) = -y \frac{\delta^2 \nu}{\delta x^2} = -y \frac{PL - Px}{EI} \quad (4.3)$$

$y$  is the distance from the neutral axis of the beam, i.e. half of the thickness (1 mm). At the points where the Bragg gratings are applied, the following deformations are obtained:

- Interlock: 223  $\mu\epsilon$ ,
- Free end: 118  $\mu\epsilon$ .

The values obtained with the simulation in Patran, with the optical fiber and with the beam theory of Eulero-Bernoulli are summarized below:

Grid position	Patran model	Optical fiber	Eulero-Bernoulli
Displacement	11 mm	-	12.5 mm
Interlock	210 $\mu\epsilon$	235 $\mu\epsilon$	223 $\mu\epsilon$
Free end	102 $\mu\epsilon$	120 $\mu\epsilon$	118 $\mu\epsilon$

Table 4.2. Summary of results between Patran model and fiber optics with Bragg gratings and the theory of the elastic line

### 4.3.2 Optical lever

The experiment of the optical lever was carried out to further confirm the results obtained with the model on the Patran software; in particular, a laser was hooked to the free end of the plate, the laser points to a wall at a distance of  $d=368$  cm. The points are marked before (point A) and after the application of the load (point B) and their distance is equal to a  $\Delta L=20$  cm, figure 4.3.2.

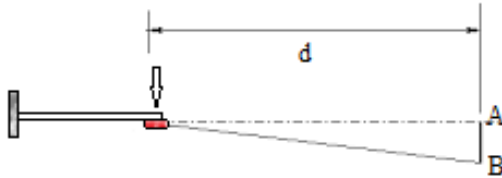


Figure 4.9. Optical lever test scheme, the laser is indicated in red

The  $\Delta L$  must be equivalent to a certain  $\Delta L_p$  (Patran) found with the simulation values:

$$\nu + \alpha d = \Delta L_p = \Delta L$$

Where  $\nu$  is the displacement and  $\alpha=0.0481$  rad is the rotation at the free end found with the simulation with Patran, in particular:  $\Delta L_p=18.8$  cm. The values can be considered comparable, taking into account a percentage of error both in the measurement of points A and B, and that the laser was attached under the plate with a rubber band and may have moved slightly.

In conclusion, the results obtained with optical fiber are comparable with the results obtained with Patran, elastic line theory and optical leverage. In the analysis, it is necessary to take into account the boundary conditions that may influence the data with errors. In particular, it should be remembered that the load is applied by hand by means of a clamp, the ageing process of the glue may have lifted the fiber from the surface of the plate; all these aspects will be analysed in the conclusions and future developments section. The results from the In-C sensor will be analysed below.

#### 4.4 In-C sensor results

As anticipated in the introduction to this chapter, the main difficulty was to compare the data coming from the In-C sensor and the optical fiber, since the first provides an average of the deformation value that occurs on the portion of the plate on which it is bonded; the second provides a measure of point deformation based on where the Bragg grating is positioned. The RF-Monitor software produces a database of data taken during the tests and represents them by means of a graph that presents the LSB (least significant bit) data in the y-coordinates and the time in the x-coordinate, as can be seen in the following figure.

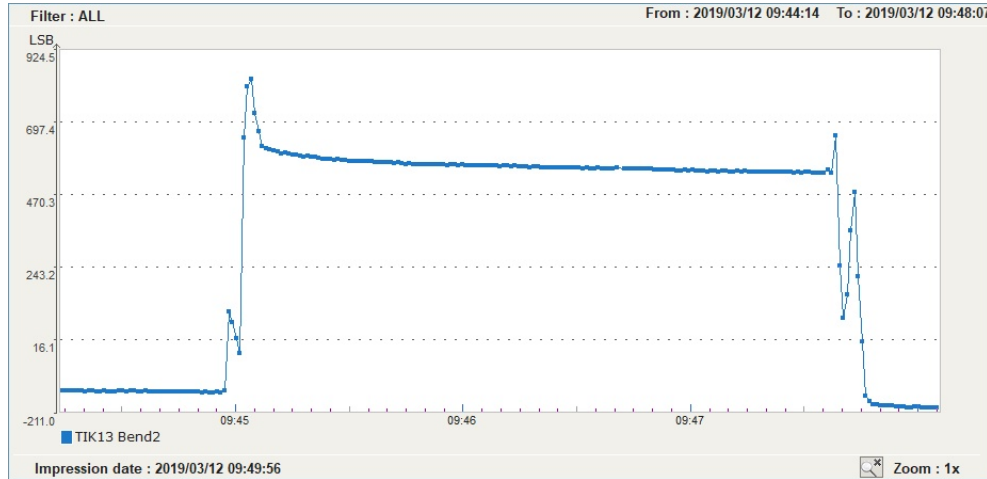


Figure 4.10. Graphic representation of the data measured by the In-C sensor during the tests

The peaks that can be seen in the graph represent the points where the load is added and removed; they are quite evident because the load is positioned by hand and if it is not particularly careful it may create large vibrations that need a longer transient phase to balance. To convert the LSB values into microstrains, data from a previous experiment were taken and interpolated to determine the coefficients of the calibration curve. By converting the data we achieve the same trend of the LSB values (figure 4.4), but, as it's possible to notice from the blue curve of figure 4.4, the deformation value in the period of application of the load is about double that resulting from the tests described previously: approximately  $500\mu\epsilon$ . Since the trend is in agreement with the strain trend in figure 4.3 (optical fibre results) it was deduced that the data used to create the calibration curve belonged to another sensor, so the trend is proper up to multiplication by a constant. This constant depends on the sensor used, each sensor has its own calibration curve; in our case the data are about double so it should be equal to  $\frac{1}{2}$ , but it is necessary to compute the calibration curve precisely with a dedicated experiment. In fact, as the graph below shows, multiplying the blue curve by  $\frac{1}{2}$  you get the trend in purple, whose average data is equal to the results obtained with the calculations and tests on the optical fiber.

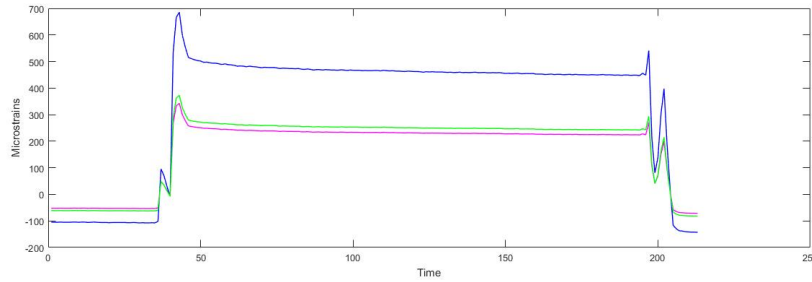


Figure 4.11. Comparison of the trend of the deformations transformed by coefficient (in purple) and by the calibration curve (in blue and in purple) that binds LSB and microstrain

It is possible to proceed in another way to determine the strain from the LSB data: otherwise, a coefficient is extracted from the ratio between the average deformation obtained from the optical fiber (table 4.2) and the average value of the measurements taken by the In-c sensor. The result is represented by the green curve in the graph above; the strain value is slightly higher than the purple curve, but it depends on the accuracy of this coefficient and on the number of data taken during the test: if the average is calculated with a limited number of data, the coefficient will be less specific than the one calculated with a higher number of data. This coefficient depends on whether you change the sensor. The outcomes described in this paragraph have been obtained using the Strain2 program, which can be viewed in Appendix B.

## 4.5 Conclusions and future developments

After a series of tests, it was reached the conclusion that the two sensors are actually comparable; below are the improvements and recommendations to achieve a more

scientifically valid result.

It is necessary, as already mentioned, to calculate a calibration curve for the type of sensor used. In addition, taking up the graph in figure 4.10, it shows a drop in the LSB value that could be caused by a failure of the adhesive that keeps the sensor fixed on the plate. There is a linear drop in the loading phase, indicated in the figure with the black markers; moreover, when the sample is unloaded, the measurements do not return to the initial condition (phase indicated by the yellow markers).

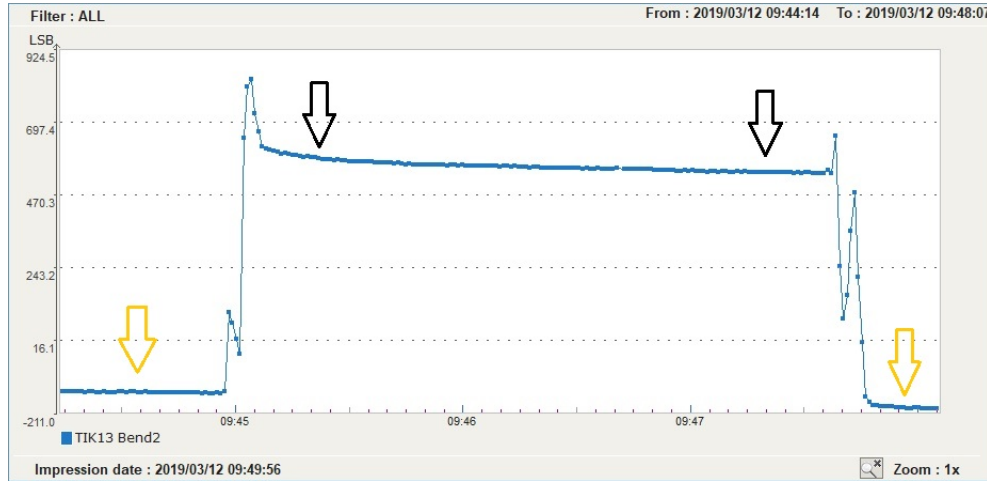
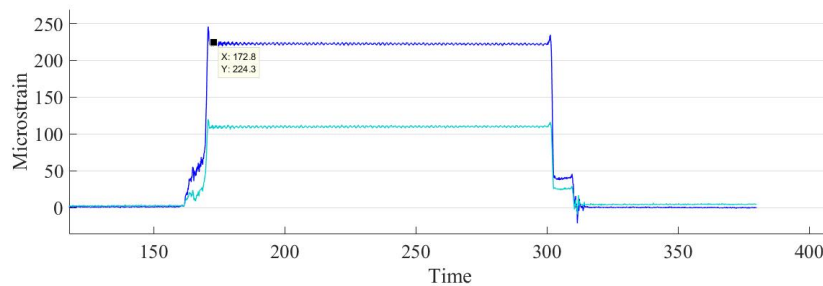


Figure 4.12. Graphic representation of the data collected by the In-C sensor

To obtain more precise data, the supports described in chapter 2 can be used and tests can be carried out with the aid of a handler so as to ensure that the load is always applied in the same place, to avoid the appearance of a twisting moment.

As far as optical fiber is concerned, it is necessary to evaluate the best bonding method to keep the fiber in contact with the surface of the component; the right quantity of glue to be used and to analyse the polymerisation and ageing times. This is because when carrying out different tests with the same load, it can be seen that the deformation value tends to increase with the course of time. As an example is reported the trend of the deformation of two tests carried out with a load of 1098 g at a distance of 1 day; in the first case the average deformation is  $224\mu\epsilon$  in the second case of  $239\mu\epsilon$ .



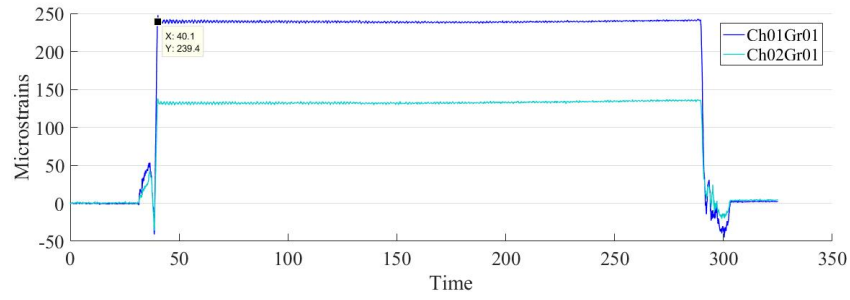


Figure 4.13. Comparison of the deformations measured by the optical fiber at a distance of 1 day

To evaluate the effective strength and stiffness of the fiber bonding, but also of the In-C sensor, it is possible to resume the tests carried out here in a couple of months.

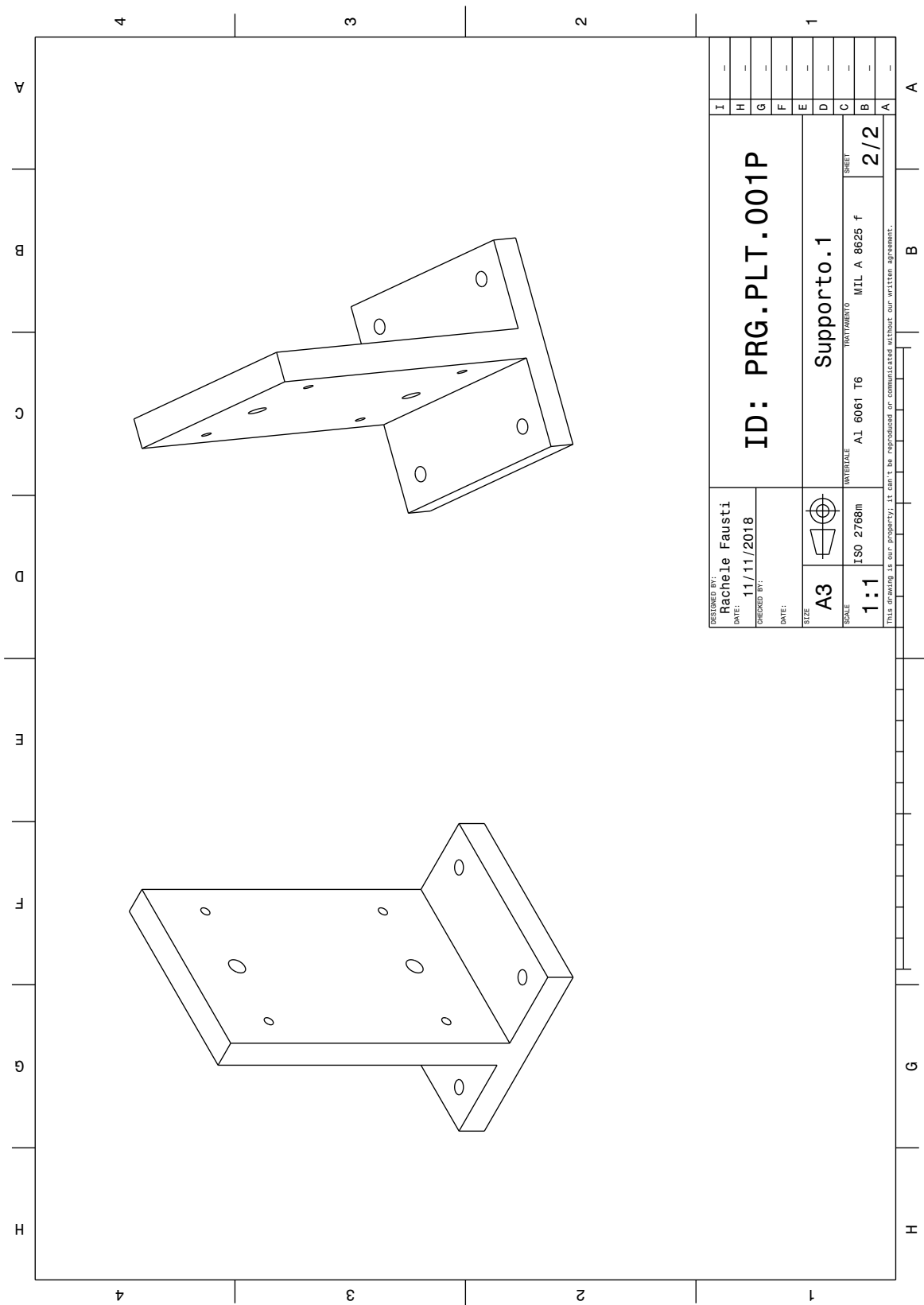
# Bibliography

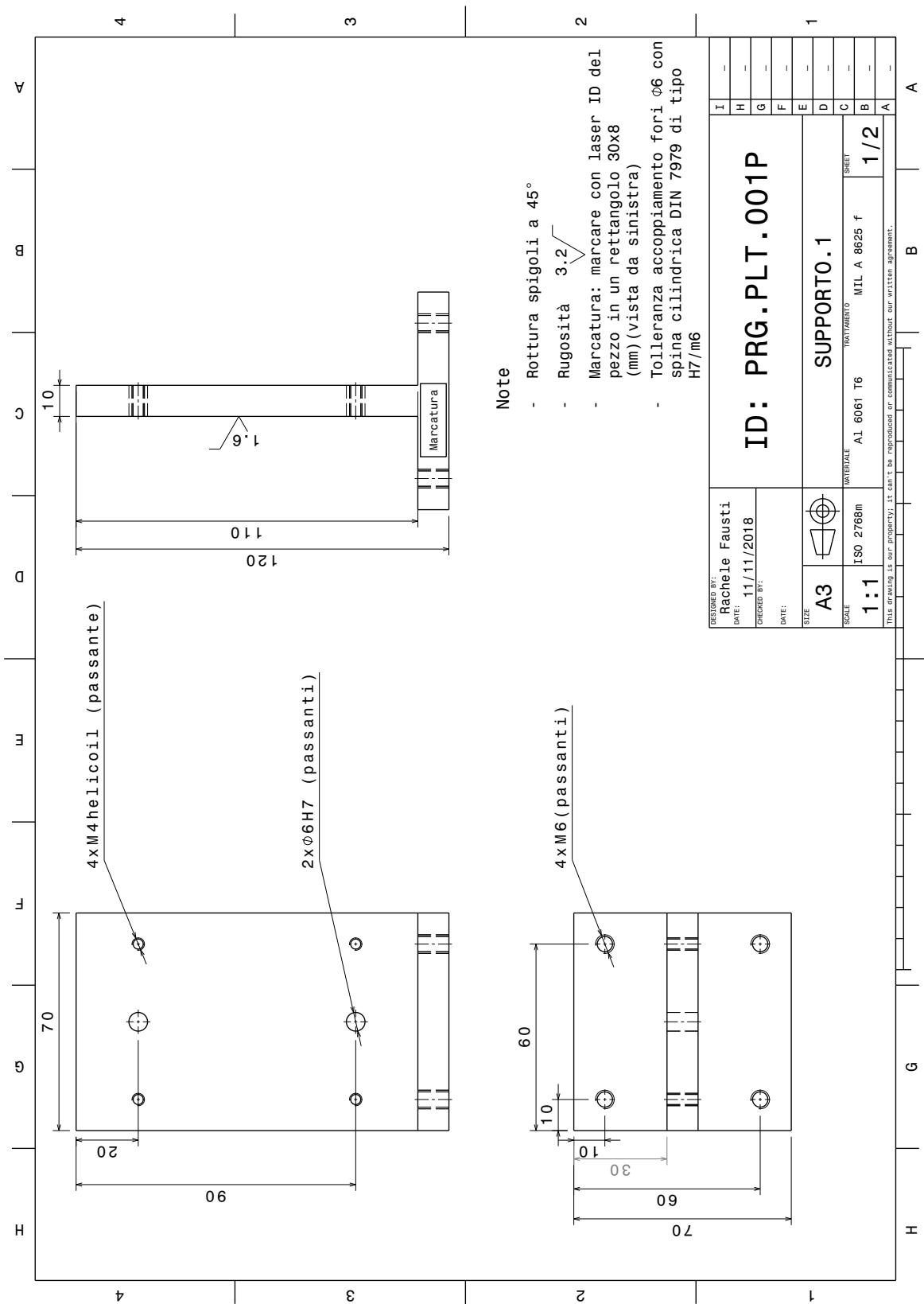
- [1] G.P. Agrawal. *Fiber Optic Communication Systems*. 2002.
- [2] M.J. Deen S. Kumar. *Fiber Optic Communications, fundamentals and applications*. 2014.
- [3] Introduction to structural health monitoring. [www.iste.co.uk](http://www.iste.co.uk)
- [4] Fiber optic sensing system (foss) monitors multiple parameters in real time. [www.nasa.gov](http://www.nasa.gov).
- [5] H. Murata. *Handbook of Optical Fibers and Cables*. 1996.
- [6] M.C. Teich B.E.A. Saleh and B.E. Saleh. *Foundamentals of Photonics*. 1991.
- [7] Nabel I. Zanoon. The phenomenon of total internal reflection and acceleration of light in fiber optics. *Internal Journal of Compute Applications*, 2014.
- [8] Guido Maisto and Marco Bonvino. Device for detecting strain and transmitting detected data and method for manufacturing the same. *US 2016/0238367*, 2016.
- [9] R. Kashyap. *Fiber Bragg Gratings*. 2009.
- [10] Teo Scolpito *Structural and thermal prognostics and diagnostic with fiber Bragg gratings*. 2018

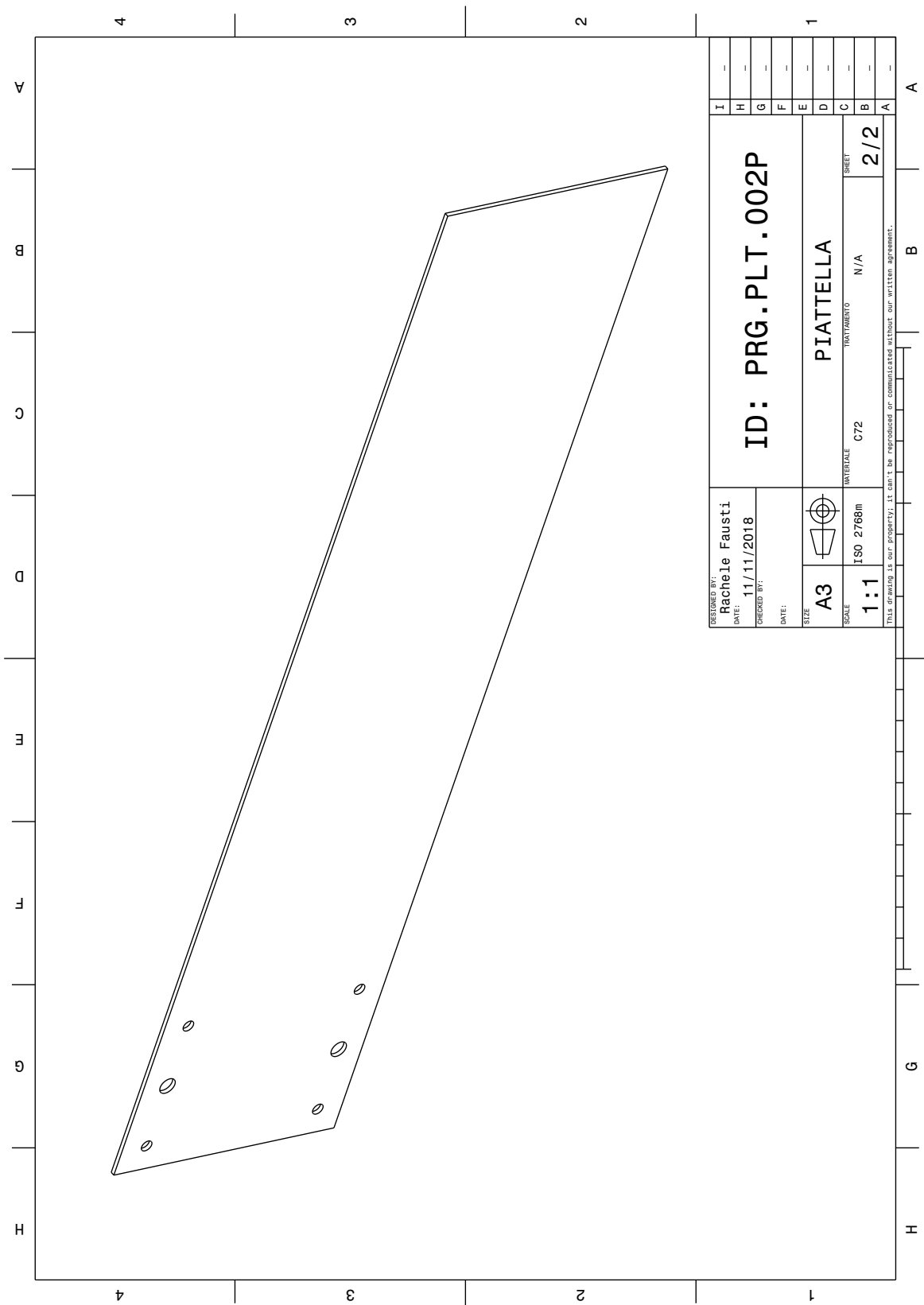
## Appendix A

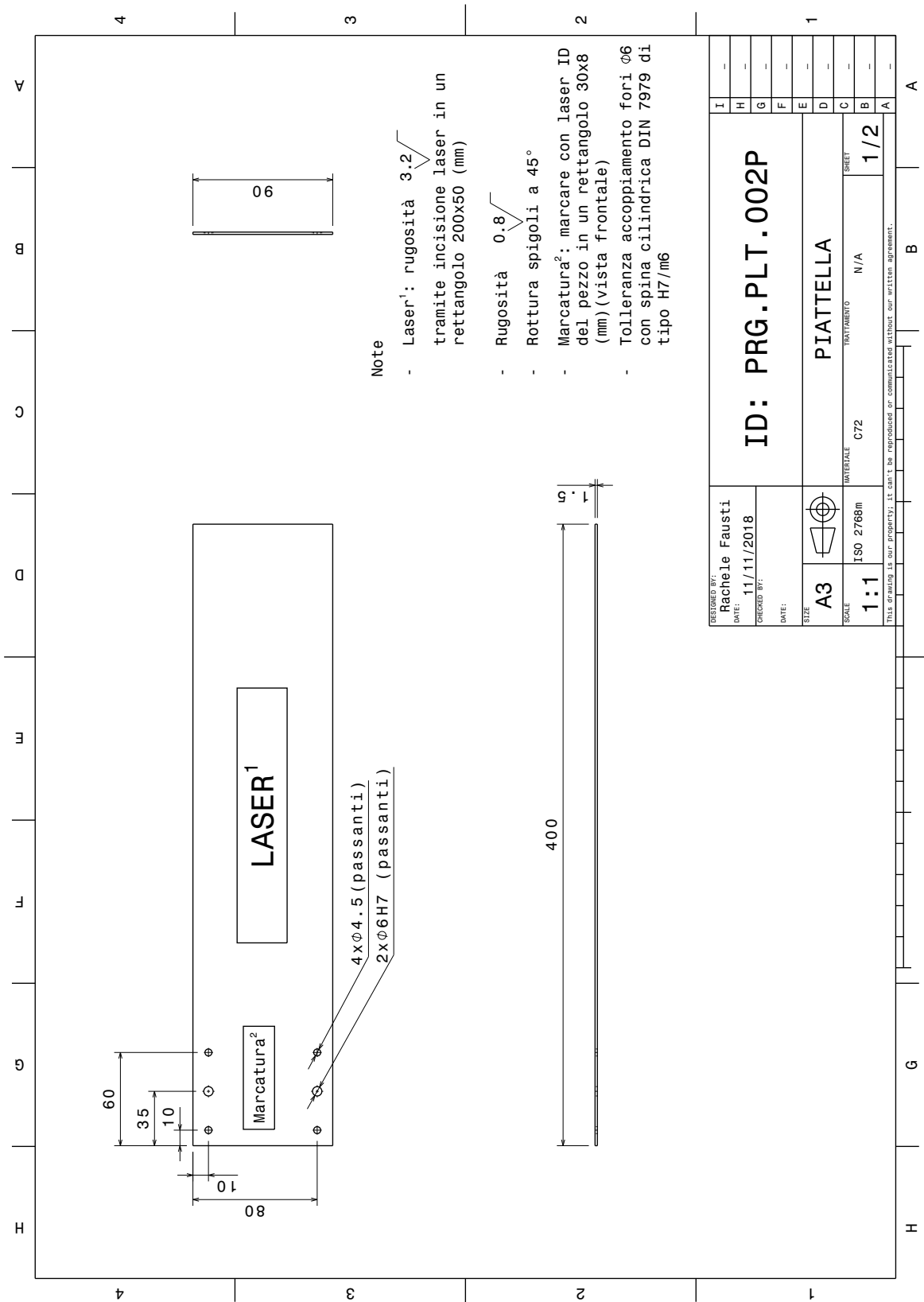
### Drawings

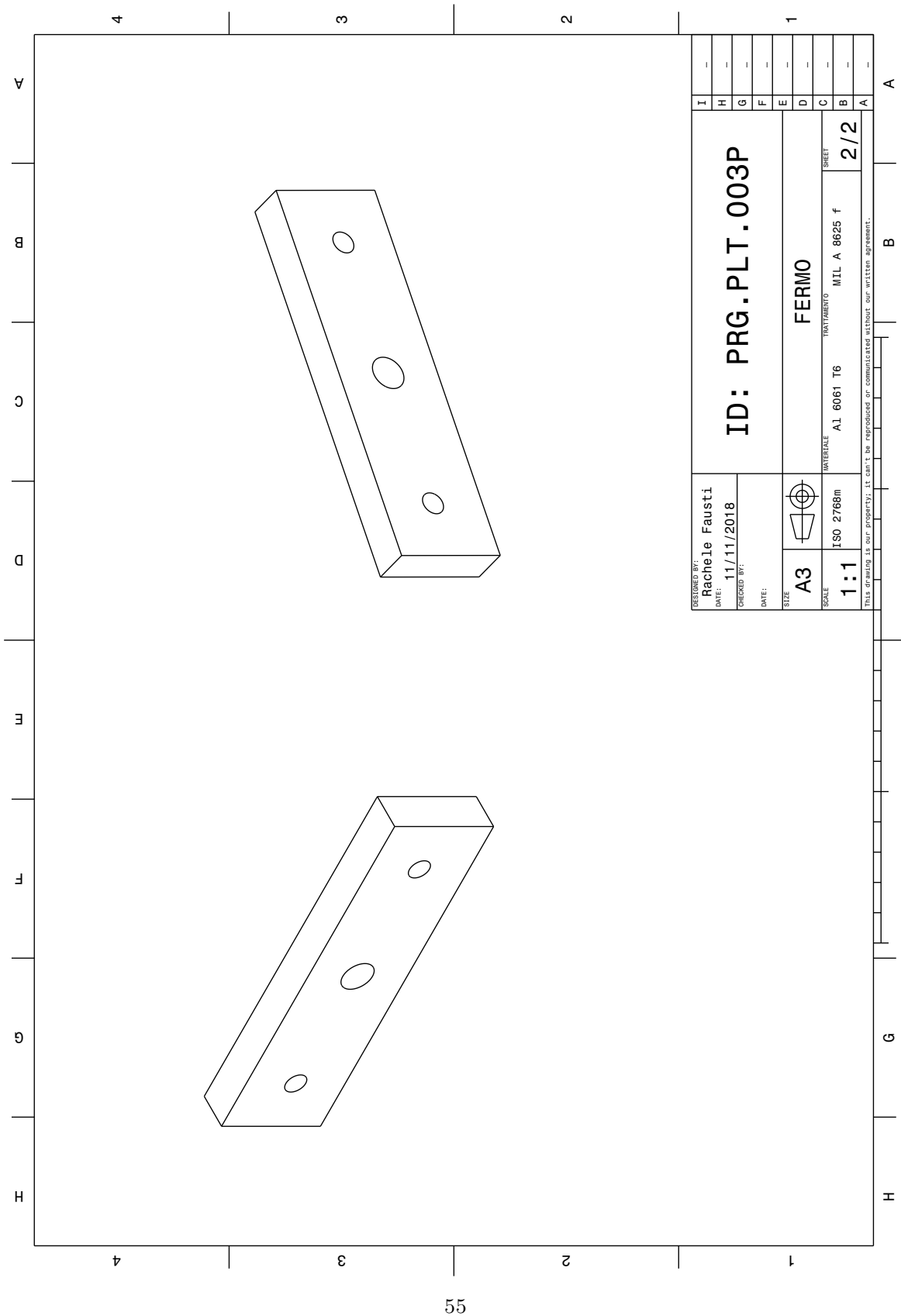


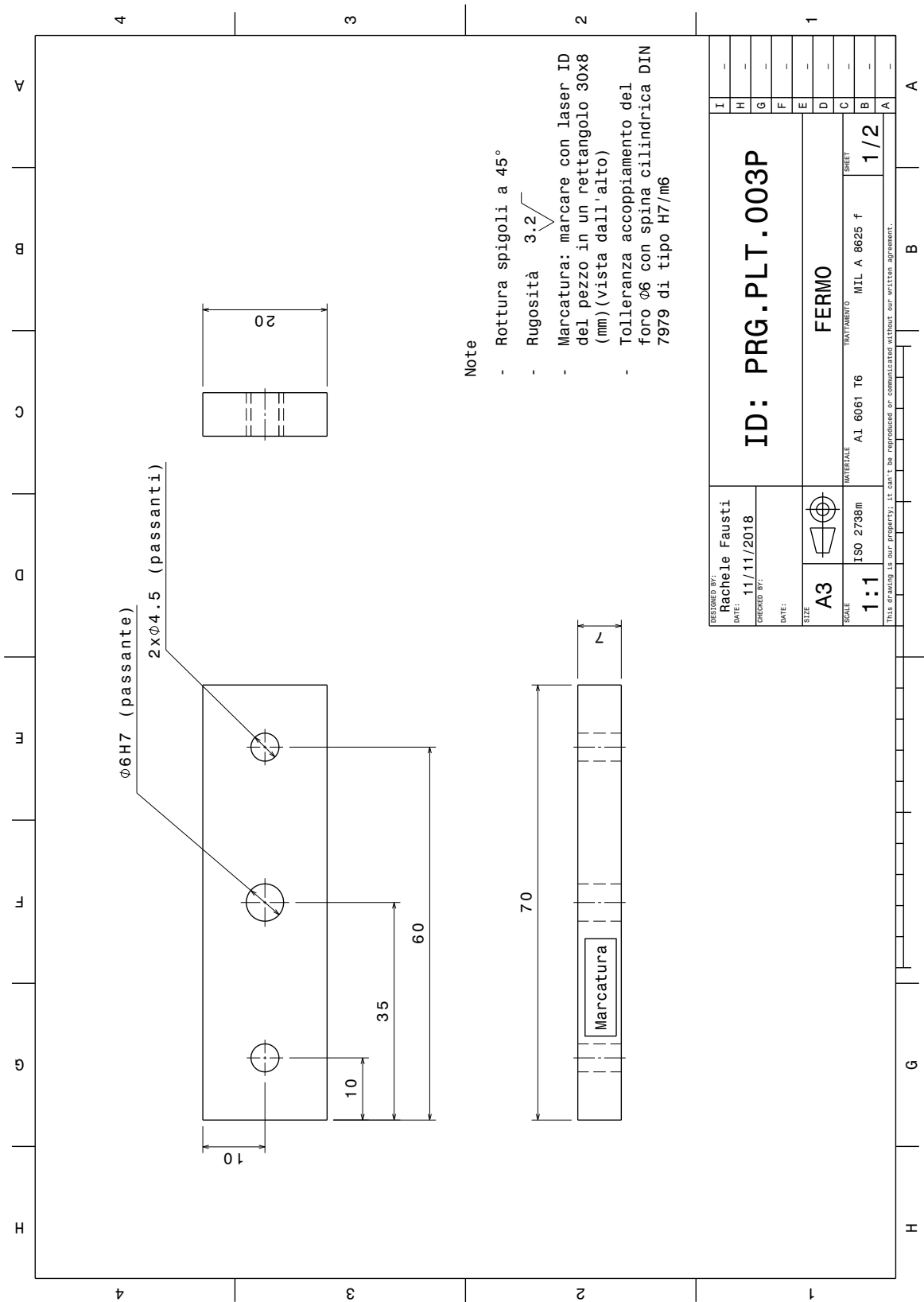


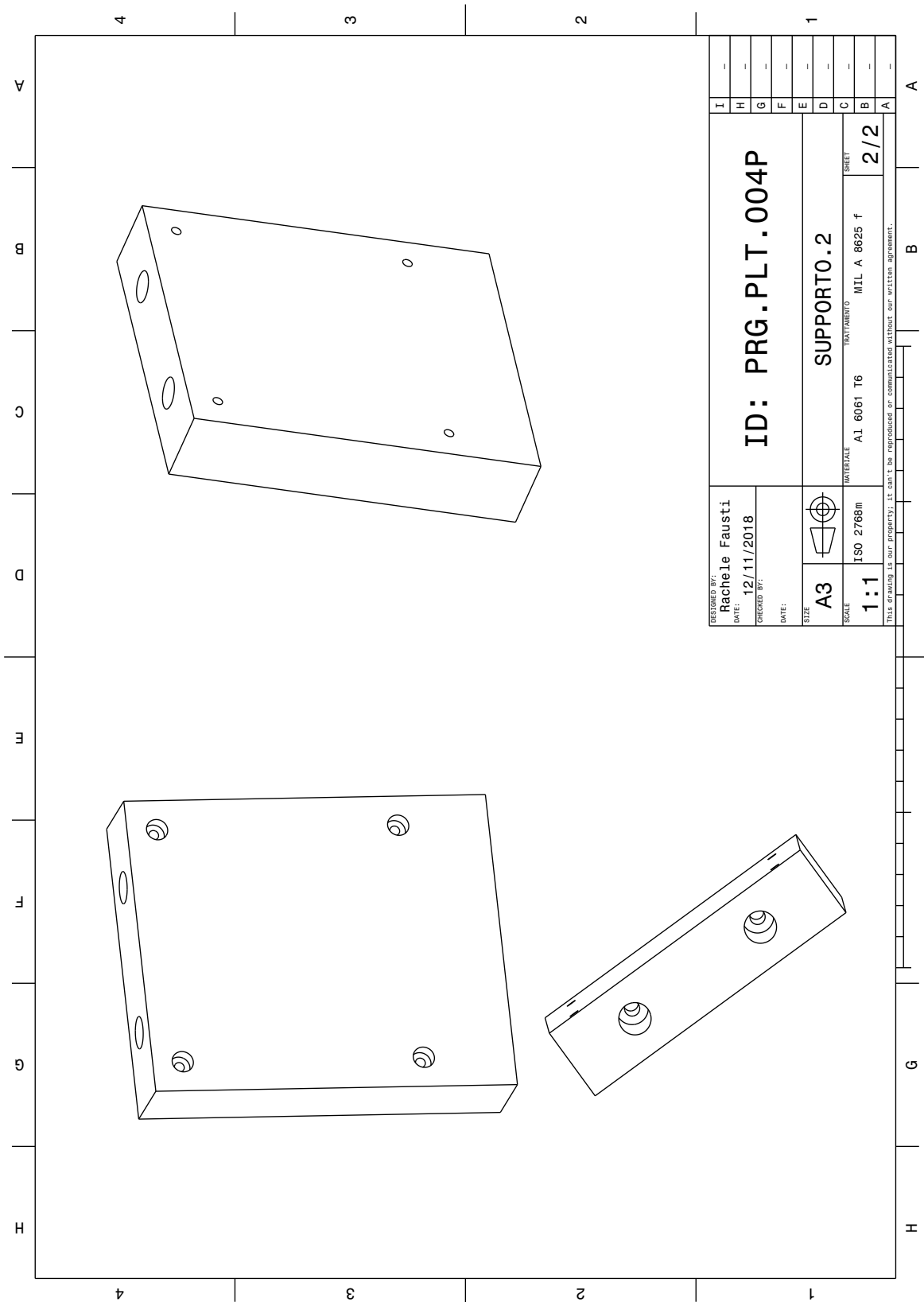


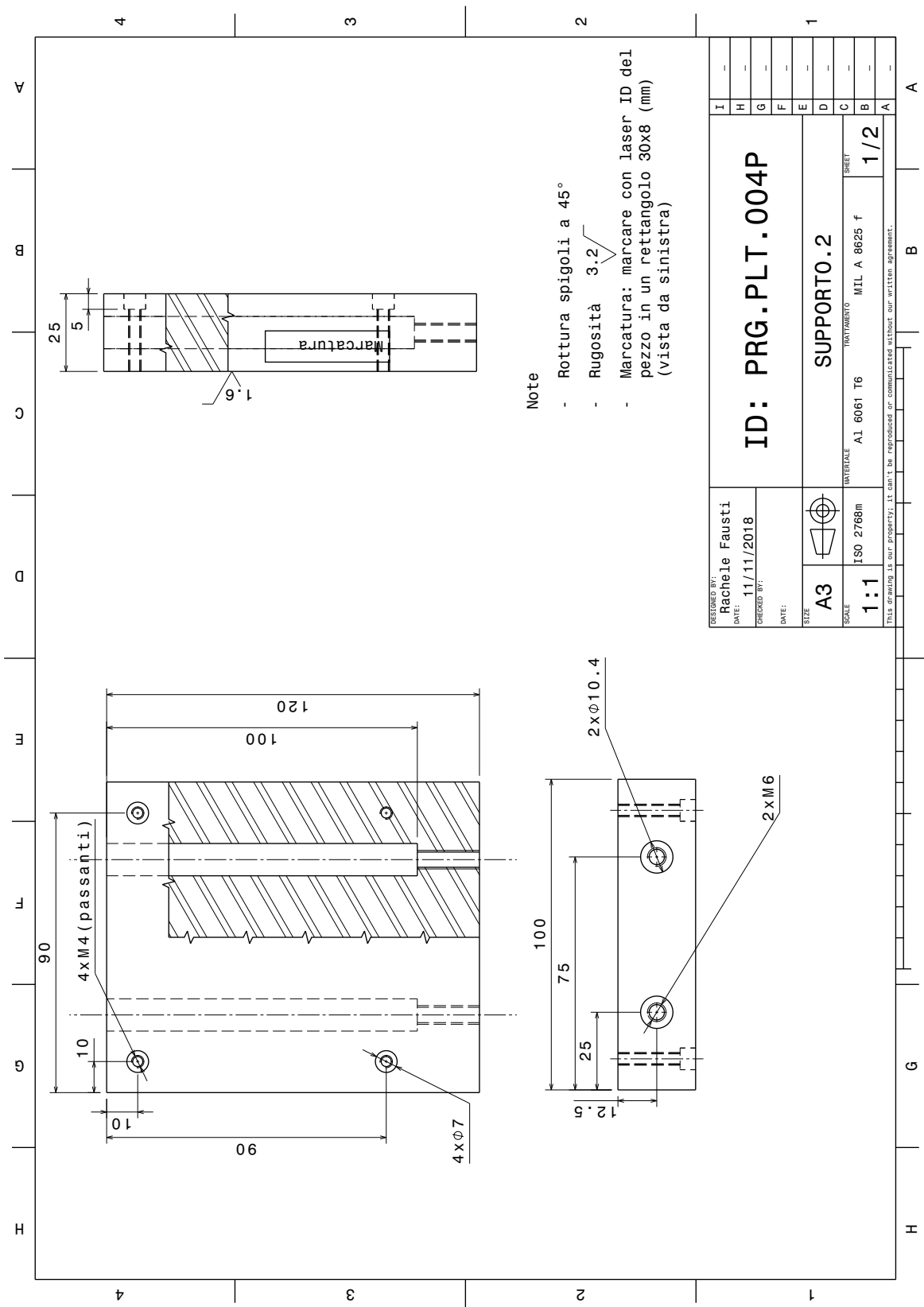




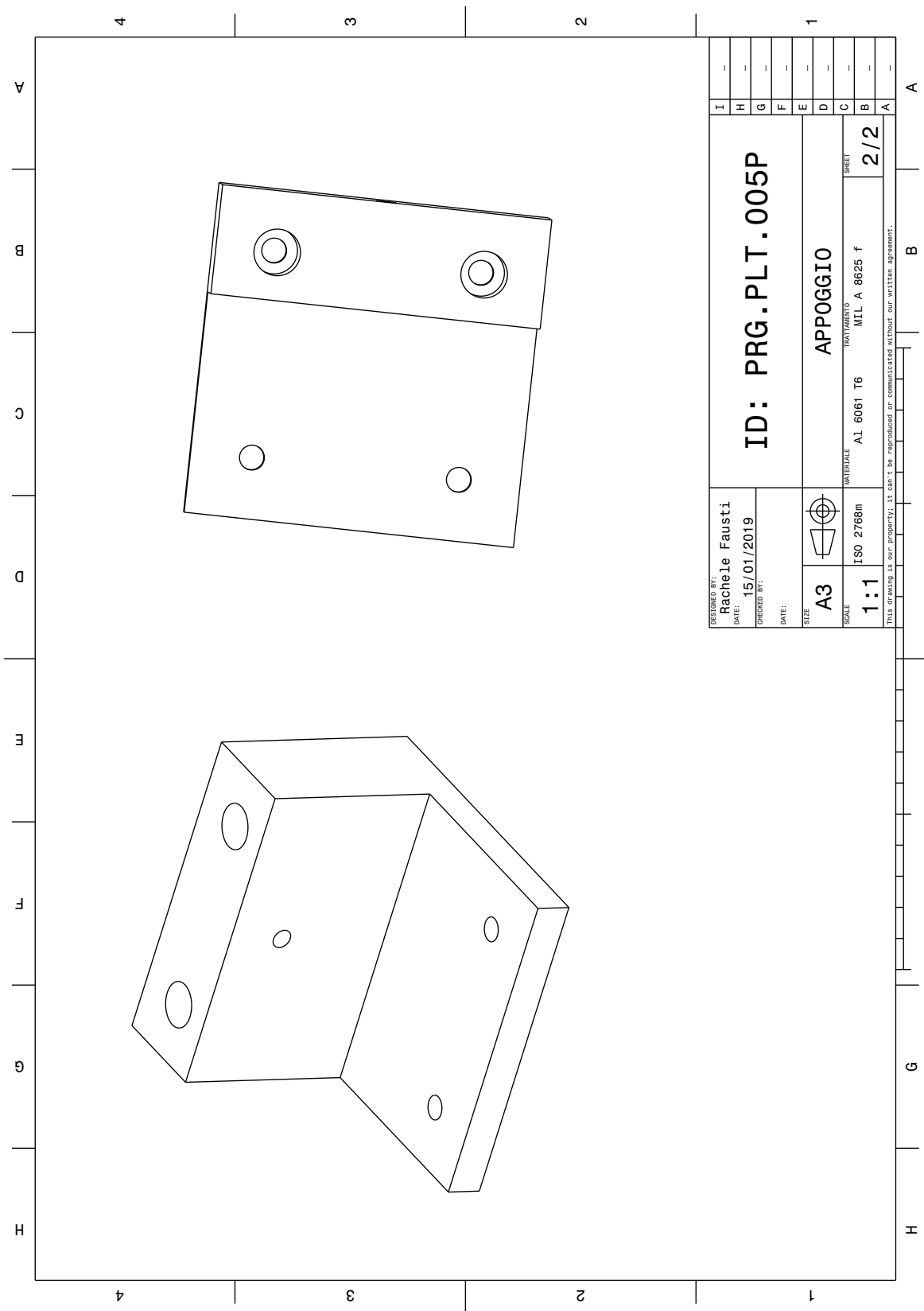




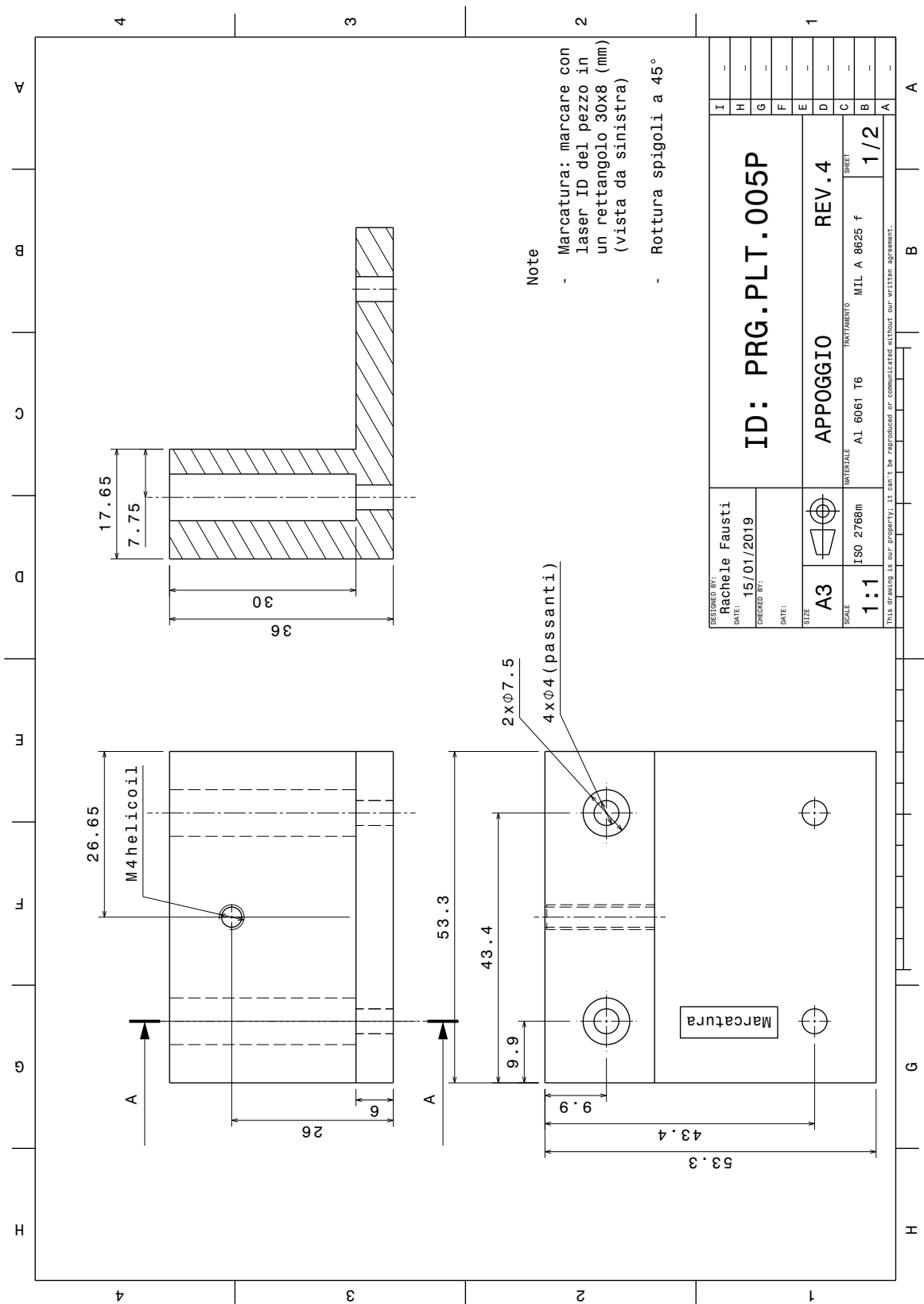


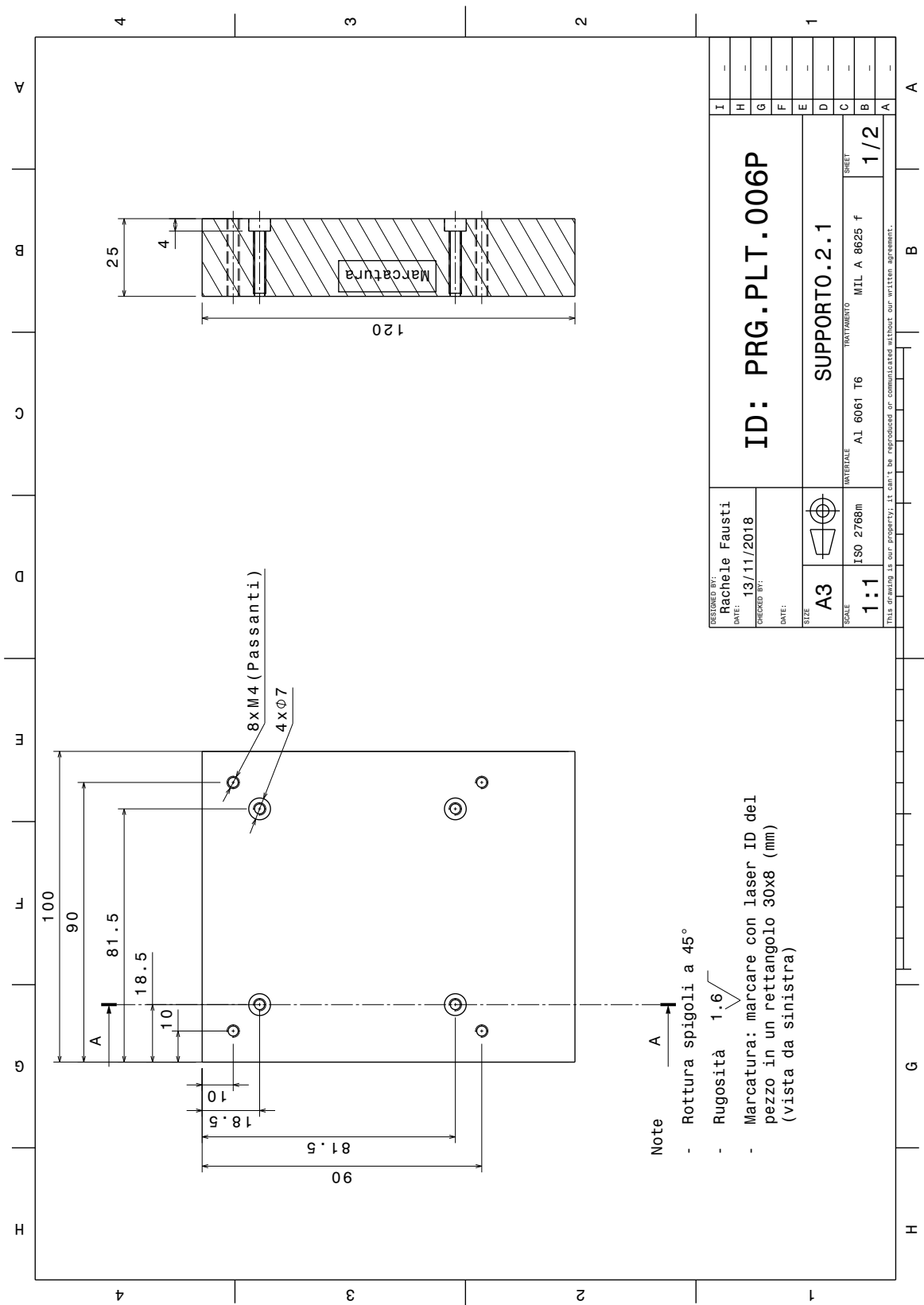


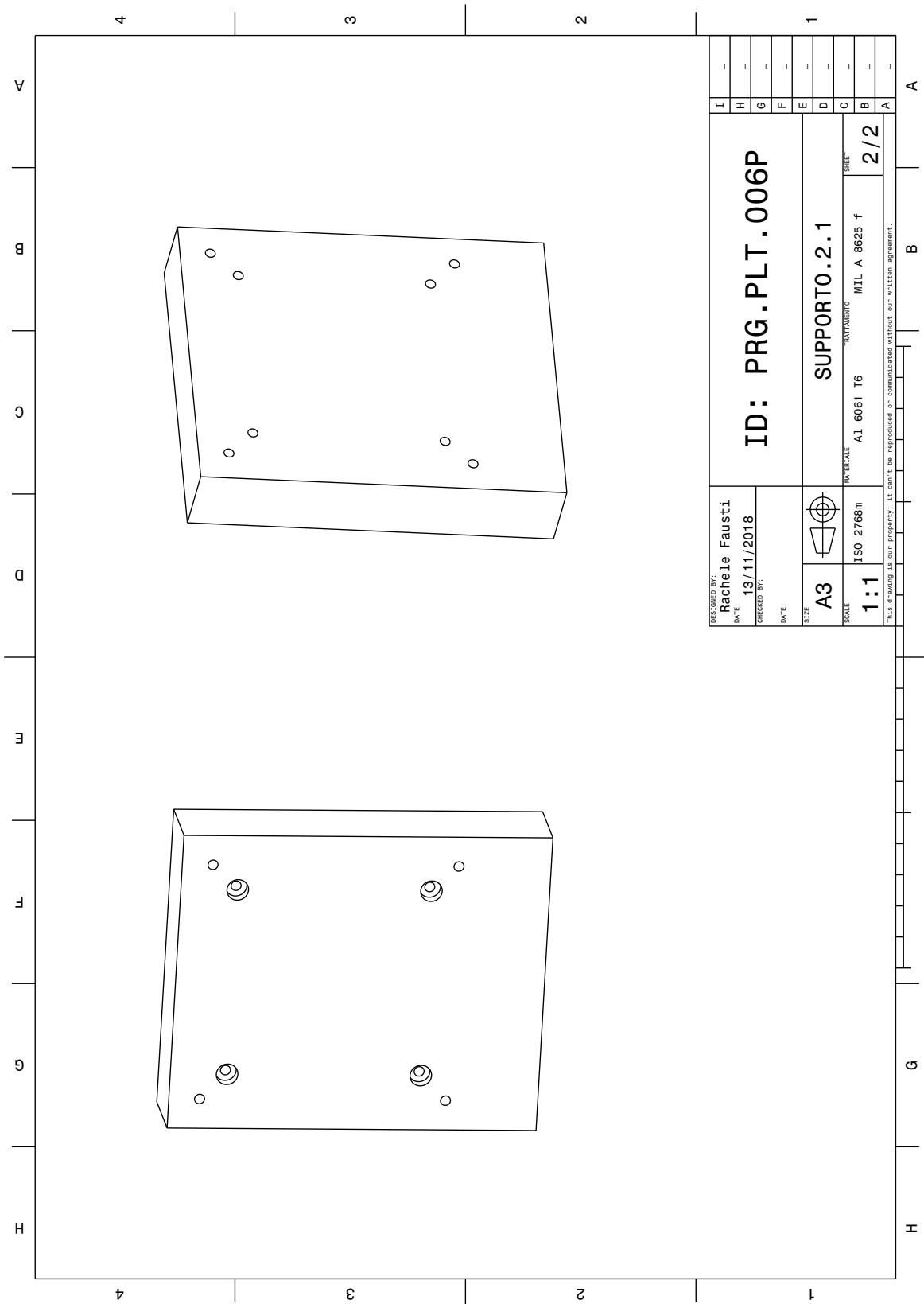


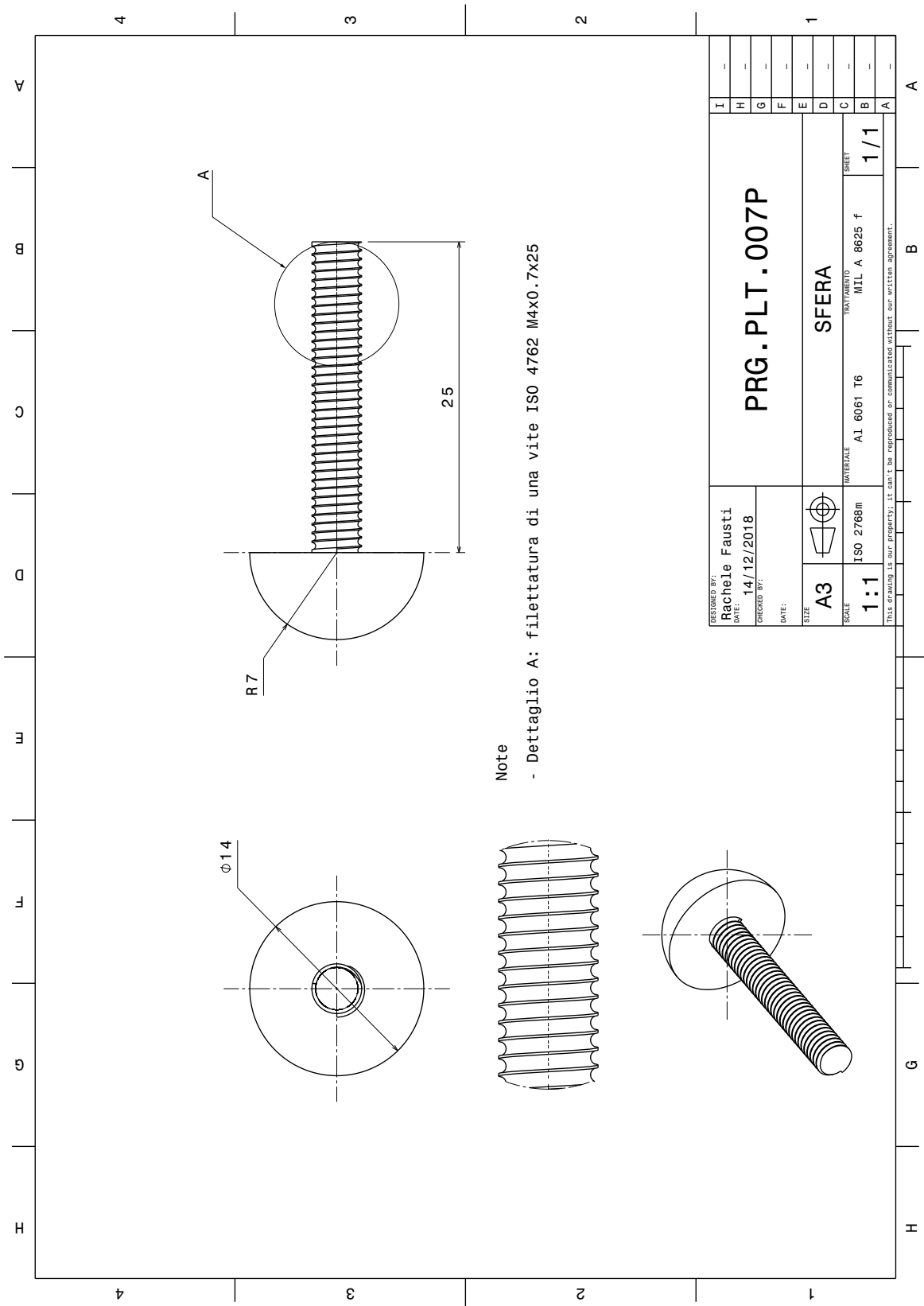


DESIGNED BY: <b>Rachele Fausti</b>	ID: PRG.PLT.005P	
DATE: <b>15/01/2019</b>		
CHECKED BY:		
DATE:		
SIZE <b>A3</b>		
SCALE <b>1:1</b>	ISO 2768m	
	MATERIALE <b>A1 6061 T6</b>	TREATAMENTO <b>MIL A 8625 f</b>
	SHEET <b>2/2</b>	
THIS DRAWING IS OUR PROPERTY; IT CAN'T BE REPRODUCED OR COMMUNICATED WITHOUT OUR WRITTEN AGREEMENT.		

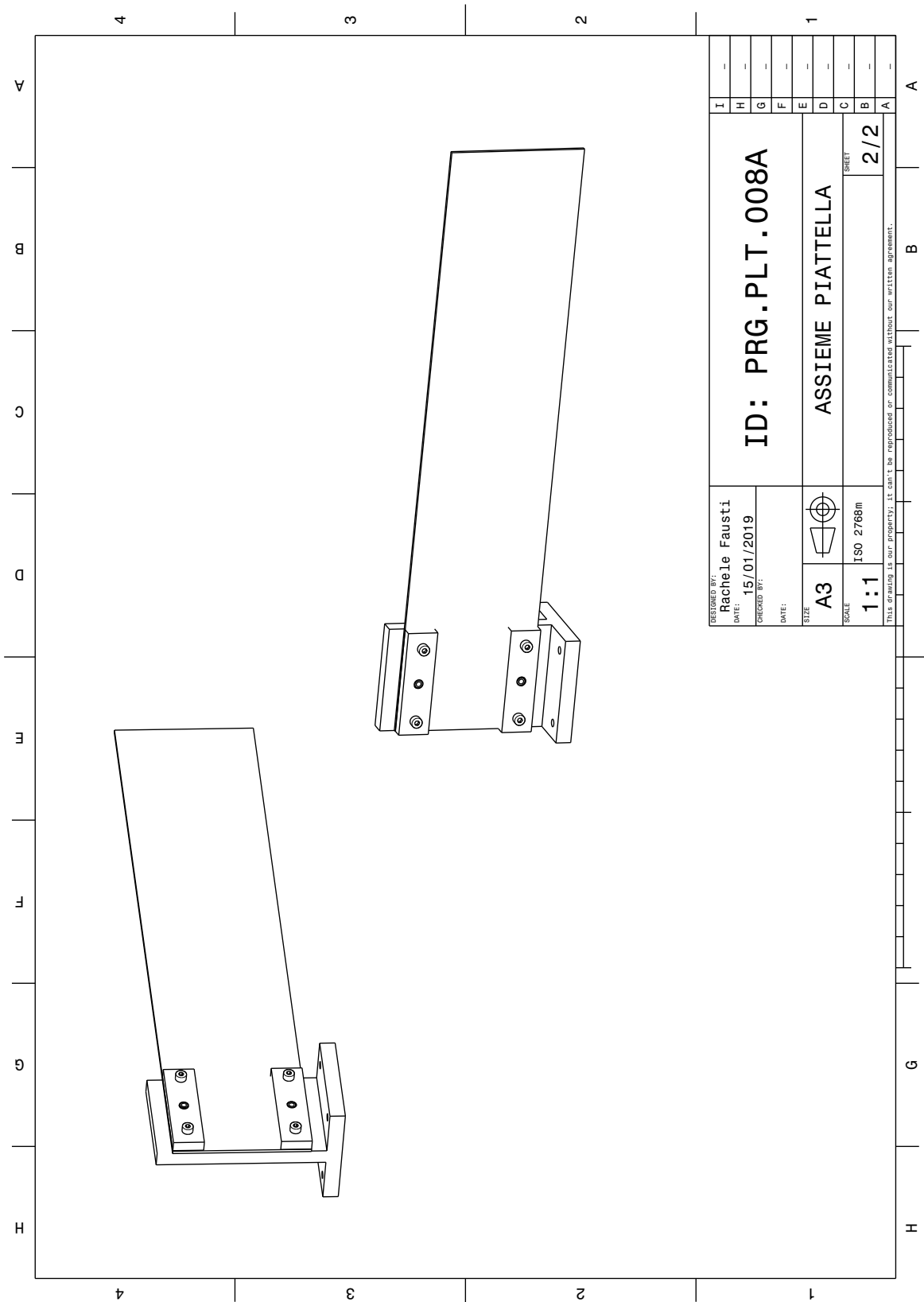


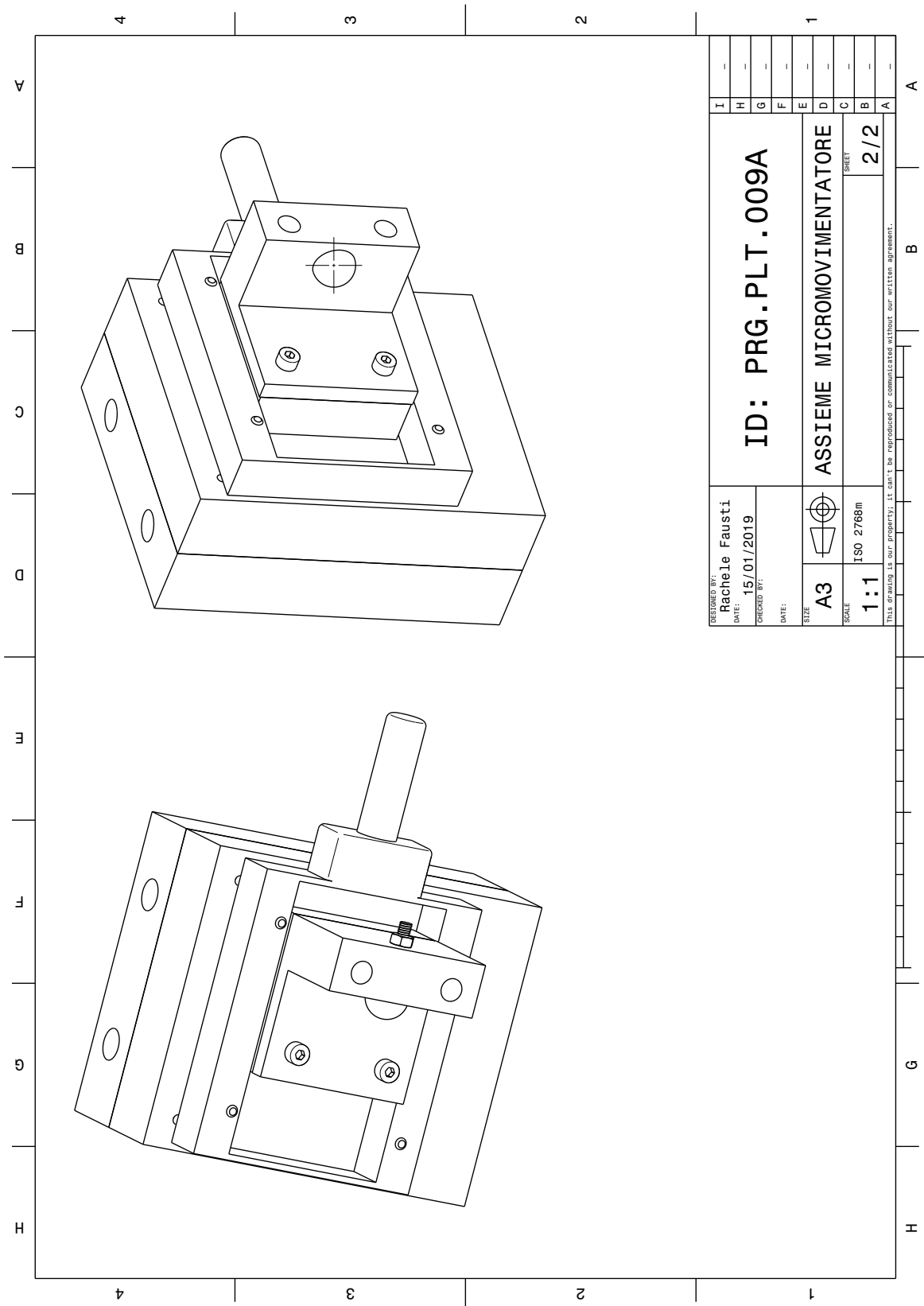




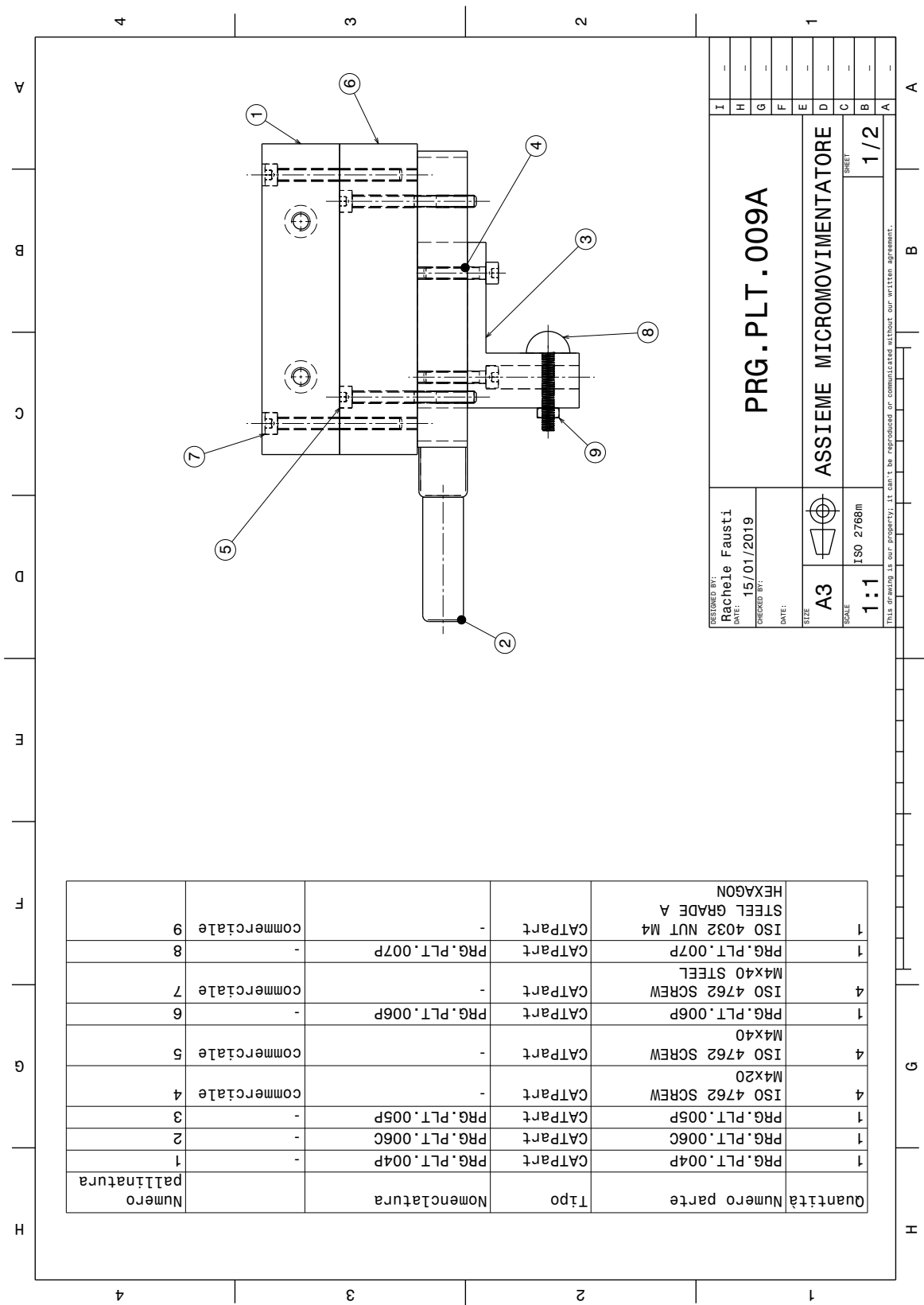


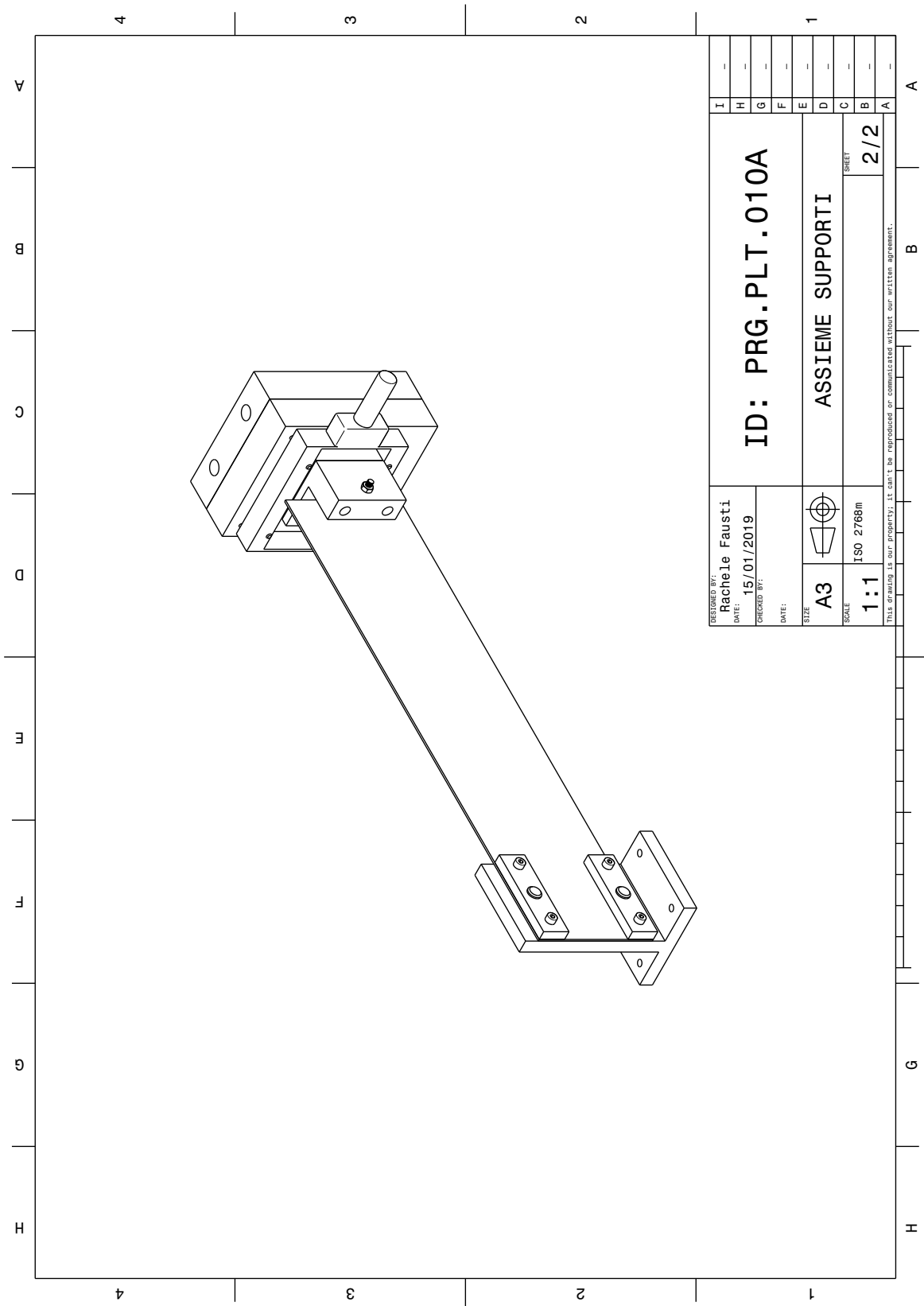







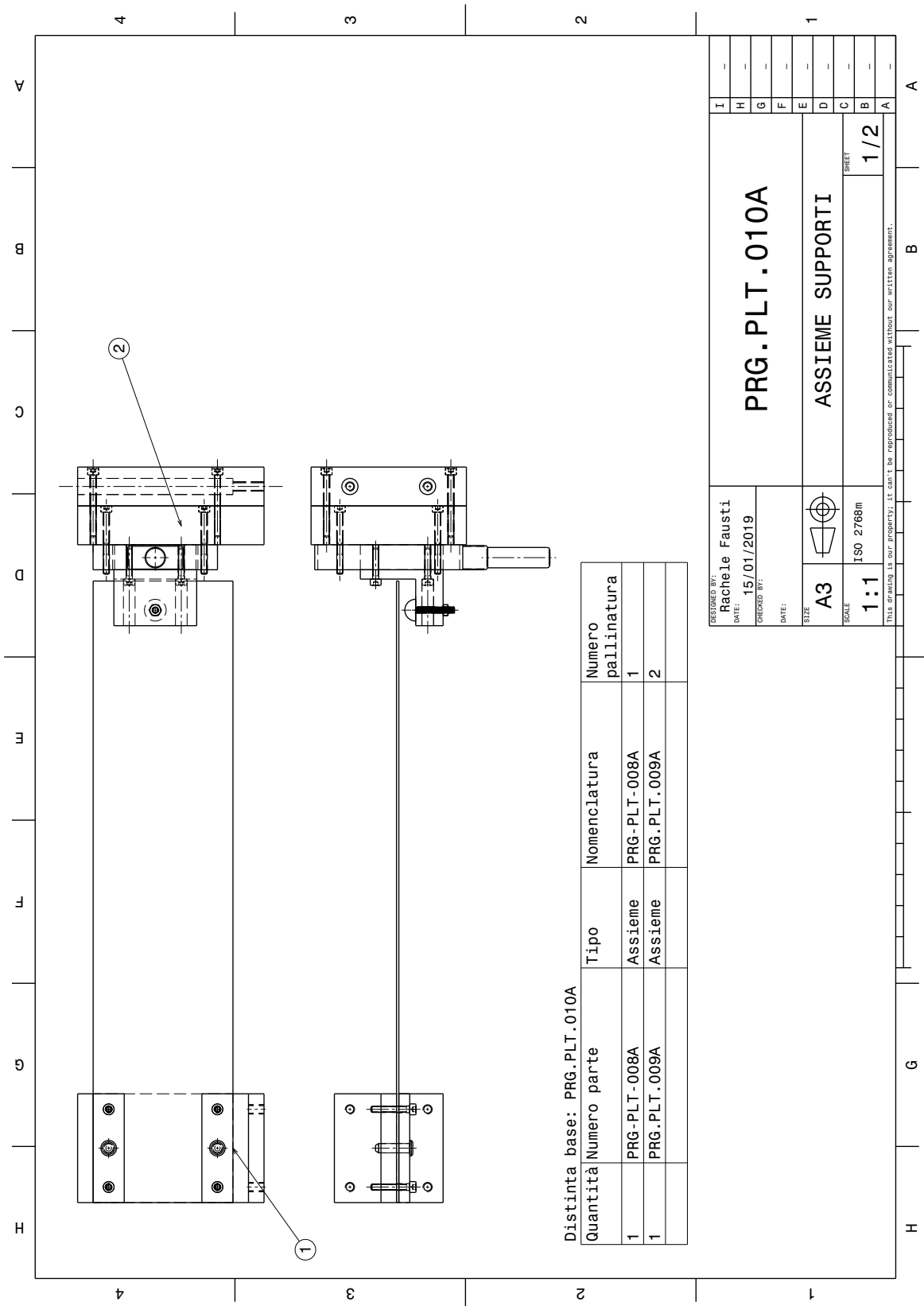






DESIGNED BY: Rachele Fausti		ID: PRG.PLT.010A		I	-
DATE: 15/01/2019				H	-
CHECKED BY:				G	-
DATE:		ASSIEME SUPPORTI		F	-
SIZE A3				E	-
				D	-
SCALE 1:1		SHEET 2/2		C	-
ISO 2768m				B	-
				A	-
THIS DRAWING IS OUR PROPERTY. IT CAN'T BE REPRODUCED OR COMMUNICATED WITHOUT OUR WRITTEN AGREEMENT.					

THIS DRAWING IS OUR PROPERTY; IT CAN'T BE REPRODUCED OR COMMUNICATED WITHOUT OUR WRITTEN AGREEMENT.



## Appendix B

### Strain2

```
clear all
close all
clc
% UTILIZZARE PER I RISULTATI IL FILE 20190301-0849_nuova2.log
%programmino che serve per estrarre il valore di strain dal file log quando
%si ha 1 solo gradino; per confrontare effettivamente quello che stampa il
%grafico dello strain con il post processing e la media dei dati presi
%direttamente dal file .log
prompt='Inserire il nome del file da importare: ';
nomefile = input(prompt,'s');
fid3 = fopen(nomefile,'r+');

%dal file .log prendiamo i dati, nel mio caso ho 3 colonne perchÃ ho la
%colonna del tempo, la colonna del primo channel e la colonna del secondo
%channel, matto tutti questi dati in una matrice matrice

i=0;
j=1;
while i<5
    riga = fgetl(fid3);
    i=i+1;
end
while ~feof(fid3)
    riga = fgetl(fid3);
    for l=1:length(riga)
        if riga(l)~','==0
            riga(l)='.';
        end
    end
    if ischar(riga)
        matrice(j,:)=str2num(riga);
```

```
j=j+1;
end
end

%b= bottom prendo tutti i valori fino a 20 secondi della fibra canale 1
b_alta = zeros(size(matrice(:,1)));
for k=1:401
    b_alta(k,1) = matrice(k,2);
end
sommab = sum(b_alta);
media_bottom_alta = sommab/401;

%t= top prendo tutti i valori tra 40 secondi a 70 secondi della fibra 1
t_alta = zeros(size(matrice(:,1)));
for k=601:1001
    t_alta(k,1) = matrice(k,2);
end
sommatt = sum(t_alta);
media_top_alta = sommatt/401;

%stessa cosa con canale 2
b_bassa = zeros(size(matrice(:,1)));
for k=1:401
    b_bassa(k,1) = matrice(k,3);
end
sommabb = sum(b_bassa);
media_bottom_bassa = sommabb/401;

t_bassa = zeros(size(matrice(:,1)));
for k=601:1001
    t_bassa(k,1) = matrice(k,3);
end
sommatt = sum(t_bassa);
media_top_bassa = sommatt/401;

%trovo valore di strain

strain_alta = (media_top_alta-media_bottom_alta)/(media_bottom_alta*(1-0.22));
strain_bassa = (media_top_bassa-media_bottom_bassa)/(media_bottom_bassa*(1-0.22));
media_valore_strain = (strain_alta+strain_bassa)/2;
%l'intervallo di tempo in cui faccio la media deve essere uguale quindi in
%ogni gradino prendo lo stesso numero di valori

%%
% MEDIA DATI CHE ESCONO DA PATRAN cambiare il peso su patrn a 1098.2 gr
bragg_patran = [0.000209 0.000211 0.000211 0.000209      0.000210 0.000103 0.00010
b = zeros(size(bragg_patran));
b(1:5,1)=bragg_patran(1:5,1);
summ = sum(b);
media = summ/5; %FIBRA ALTA
```

```
c = zeros(size(bragg_patran));
c(6:10,1)=bragg_patran(6:10,1);
summ2 = sum(c);
media2 = summ2/5 ;%FIBRA BASSA

%%

time = zeros(size(matrice(:,1)));

for k=1:2226
time(k,1)= matrice(k,1);
end
media_vett = zeros(size(matrice(:,1)));
media2_vett = zeros(size(matrice(:,1)));
strain_alta_vett = zeros(size(matrice(:,1)));
strain_bassa_vett = zeros(size(matrice(:,1)));

media_vett(:,1)= media*10^6;
media2_vett(:,1)= media2*10^6;
strain_alta_vett(:,1)= strain_alta*10^6;
strain_bassa_vett(:,1)= strain_bassa*10^6;

%% Import the data

[~, ~, raw] = xlsread('C:\Users\User\Desktop\TESI\File.Tesi\ProveTesi\20190311_d

%% Create output variable
datiegraficisensori = reshape([raw{:}], size(raw));

%% Clear temporary variables
clearvars raw;

xdati(:,1) = -datiegraficisensori(:,2);
ymicros(:,1)= datiegraficisensori(:,1);

P = polyfit(xdati,ymicros,1);
retta=polyval(P,xdati);
%plot(xdati,retta,'o')
%% importo i dati num2
val_nuova2 = xlsread('C:\Users\User\Desktop\TESI\File.Tesi\ProveTesi\DatabaseRepo

%% Clear temporary variables
clearvars raw;
%UTILIZZO LA RETTA
micros_nuova2 = polyval(P,val_nuova2);
time2=1:213;

microstrain_nuova2 = micros_nuova2/2;
```

```
% inc = zeros(213,1);
% for k=18:118
%     inc(k,1)=microstrain_nuova2(k,1);
% end
% somma = sum(inc);
% media_inc=somma/100;

%MEDIA DEI VALORI DEL SENSORE INC
media_val_nuova2 = mean(val_nuova2);

%RAPPORTO VALORE DI STRAIN MEDIO E MEDIA DEI VALORI DEL SENSORE
COEFF = media_valore_strain/media_val_nuova2;
%USO COEFFICIENTE
microstrain_coeff = zeros(size(val_nuova2));
for k=1:213
microstrain_coeff(k,1)=COEFF*val_nuova2(k,1)*10^6;
end

%PLOT RISULTATI RETTA/2 e COEFF
figure(1)
plot(time2,micros_nuova2)
hold on
plot(time2,microstrain_nuova2)
hold on
plot(time2, microstrain_coeff)

%PLOT MEDIA STRAIN TRA PATRAN E SCRIPT
figure(3)
plot(time,media_vett,'b')
hold on
plot(time,media2_vett,'b')
plot(time,strain_alta_vett,'r')
plot(time,strain_bassa_vett,'r')

%% prova se funziona il coeff con i dati di prova 1A

%prendere i dati di inc moltiplicarli per COEFF e vedere se vengono circa
%lo strain del file .log

[~, ~, raw] = xlsread('C:\Users\User\Desktop\TESI\File.Tesi\ProveTesi\Prova1A.xls');

IN_C_1A = reshape([raw{:}],size(raw));

clearvars raw;

time_1A=1:315;
%CON RETTA E DIVISO 2
micros_1A = polyval(P,IN_C_1A);
microstrain_1A = micros_1A/2;
```

```
%CON COEFF
microstrain_coeff_1A = zeros(size(IN_C_1A));
for k=1:315
microstrain_coeff_1A(k,1)=COEFF*IN_C_1A(k,1)*10^6;
end

figure(4)
plot(time_1A,IN_C_1A)
hold on
plot(time_1A,microstrain_1A,'g')
hold on
plot(time_1A,microstrain_coeff_1A,'c')
```